

Geology and thermochronology of Tertiary Cordilleran-style metamorphic core complexes in the Saghand region of central Iran

Charles Verdel[†]

Brian P. Wernicke

Division of Geological and Planetary Sciences, California Institute of Technology, Pasadena, California 91125, USA

Jahandar Ramezani

Department of Earth, Atmospheric and Planetary Sciences, Massachusetts Institute of Technology, Cambridge, Massachusetts 02139, USA

Jamshid Hassanzadeh

Department of Geology, University of Tehran, Tehran, Iran

Paul R. Renne

Berkeley Geochronology Center, 2455 Ridge Road, Berkeley, California 94709, USA, and Department of Earth and Planetary Science, University of California, Berkeley, California 94720, USA

Terry L. Spell

Department of Geoscience, University of Nevada, Las Vegas, Nevada 89154, USA

ABSTRACT

An ~100-km-long north-south belt of metamorphic core complexes is localized along the boundary between the Yazd and Tabas tectonic blocks of the central Iranian micro-continent, between the towns of Saghand and Posht-e-Badam. Amphibolite facies mylonitic gneisses are structurally overlain by east-tilted supracrustal rocks including thick (>1 km), steeply dipping, nonmarine siliciclastic and volcanic strata. Near the detachment (the Neybaz-Chatak fault), the gneisses are generally overprinted by chlorite brecciation. Crosscutting relationships along with U-Pb zircon and ⁴⁰Ar/³⁹Ar age data indicate that migmatization, mylonitic deformation, volcanism, and sedimentation all occurred in the middle Eocene, between ca. 49 and 41 Ma. The westernmost portion of the Tabas block immediately east of the complexes is an east-tilted crustal section of Neoproterozoic–Cambrian crystalline rocks and metasedimentary strata >10 km thick. The ⁴⁰Ar/³⁹Ar biotite ages of 150–160 Ma from structurally deep parts of the section contrast with ages of 218–295 Ma from shallower parts, and suggest Late Jurassic tilting of the crustal section. These results define three events: (1) a Late Jurassic period of upper crustal

cooling of the western Tabas block that corresponds to regional Jurassic–Cretaceous tectonism and erosion recorded by a strong angular unconformity below mid-Cretaceous strata throughout central Iran; (2) profound, approximately east-west middle Eocene crustal extension, plutonism, and volcanism (ca. 44–40 Ma); and (3) ~2–3 km of early Miocene (ca. 20 Ma) erosional exhumation of both core complex and Tabas block assemblages at uppermost crustal levels, resulting from significant north-south shortening. The discovery of these and other complexes within the mid-Tertiary magmatic arcs of Iran demonstrates that Cordilleran-style core complexes are an important tectonic element in all major segments of the Alpine-Himalayan orogenic system.

Keywords: metamorphic core complex, extensional tectonics, thermochronology, Iran, Alpine-Himalayan orogen, Arabia-Eurasia collision.

INTRODUCTION

The Cenozoic geology of Iran has traditionally been viewed in terms of two dominant events: widespread and voluminous Eocene–Oligocene primarily arc-related volcanism (e.g., Forster et al., 1972) (Fig. 1) and accompanying rapid sedimentation, and Miocene and younger folding, thrusting, and strike-slip faulting accommodating

the collision between Arabia and Eurasia (e.g., Stöcklin, 1968). More recently, some authors have proposed an Eocene to Miocene phase of crustal extension in Iran and adjacent regions to explain the local alkaline affinity of Tertiary volcanism and the onset of rapid sedimentation (Hassanzadeh et al., 2002; Vincent et al., 2005). Recognition of tectonic elements of Late Cretaceous and younger age associated with significant crustal extension in Iran has included reports of domino-style normal faulting in the Golpaygan region (Tillman et al., 1981) and rapid exhumation of mylonitic crystalline rocks along extensional detachment faults in the Takab, Biarjmand, and Posht-e-Badam areas (Stockli et al., 2004; Hassanzadeh et al., 2005; Kargaran et al., 2006, respectively; Fig. 1).

In this paper we present the results of field and analytical work in the Saghand and Posht-e-Badam area of central Iran, where we have documented a north-trending belt of domino-form mountain ranges exhibiting the traits of the mid-Tertiary metamorphic core complexes in the Sonora Desert region of southwestern North America (e.g., Davis, 1980; Reynolds, 1985). These include mylonitized, high-grade granitic rocks below a low-angle detachment fault with associated chlorite brecciation; low-grade to unmetamorphosed upper plate rocks; and a supradetachment basin containing a thick succession of scarp facies nonmarine strata. We first describe the regional and local geological

[†]cverdel@gps.caltech.edu

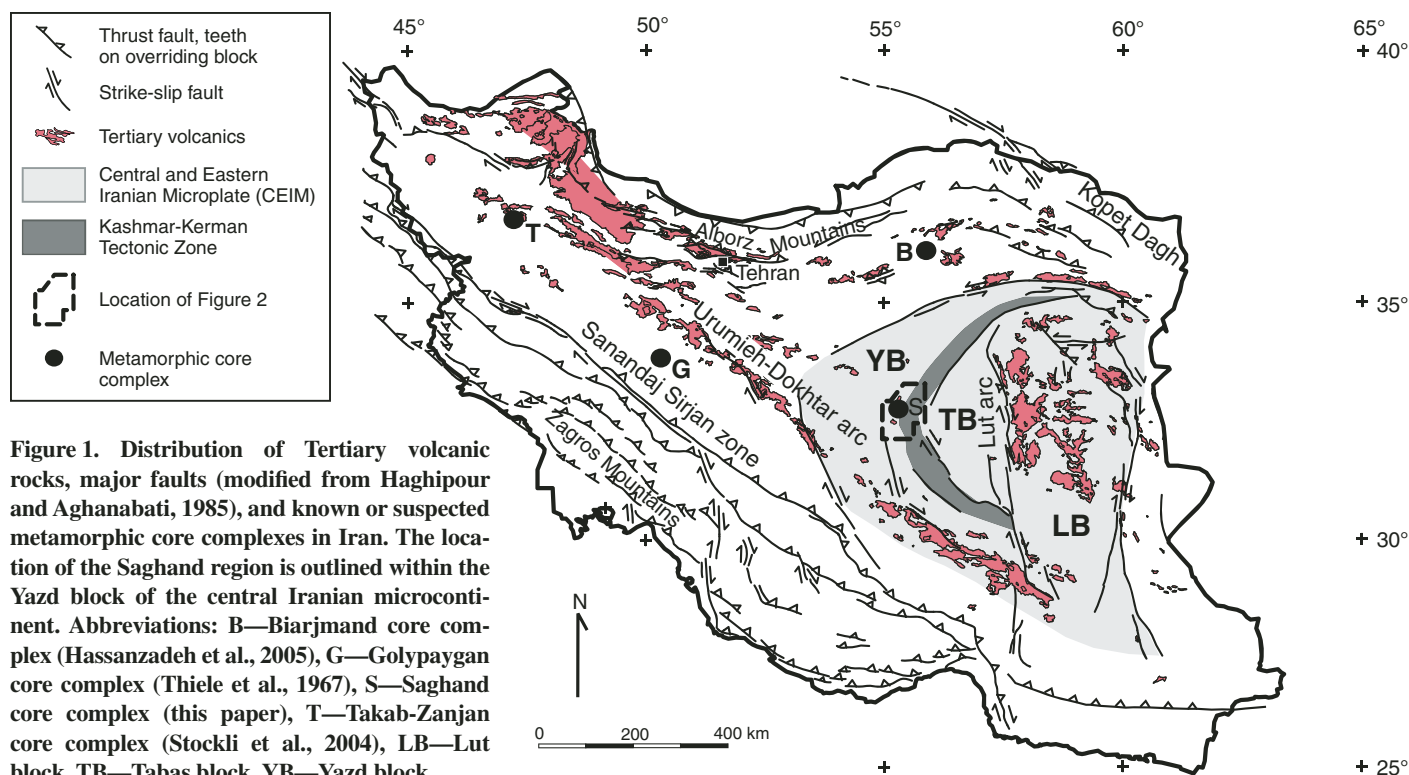


Figure 1. Distribution of Tertiary volcanic rocks, major faults (modified from Haghipour and Aghanabati, 1985), and known or suspected metamorphic core complexes in Iran. The location of the Saghand region is outlined within the Yazd block of the central Iranian microcontinent. Abbreviations: B—Biarjmand core complex (Hassanzadeh et al., 2005), G—Golpaygan core complex (Thiele et al., 1967), S—Saghand core complex (this paper), T—Takab-Zanjan core complex (Stockli et al., 2004), LB—Lut block, TB—Tabas block, YB—Yazd block.

setting of these central Iranian ranges based on previous work, and then systematically describe the extensional tectonic elements. Building on an extensive database of U-Pb geochronology of crystalline and volcanic rocks (Ramezani and Tucker, 2003), we then present new U-Pb, (U-Th)/He, and $^{40}\text{Ar}/^{39}\text{Ar}$ data that refine the timing of extensional deformation as well as earlier and later periods of major deformation, and discuss the significance of this data for the Tertiary evolution of the Tethysides.

TECTONIC SETTING

The Iranian segment of the Alpine-Himalayan orogenic system has a complex Permian–Quaternary history of successive rifting and collision, but most of Iran is underlain by a relatively concordant blanket of Paleozoic platform sediments similar to those on the Arabian platform (e.g., Stöcklin, 1968). It is therefore generally believed that the major continental blocks in Iran, as outlined by narrow belts of Mesozoic ophiolitic rocks, had a common origin in a cratonic platform along the northern flank of Gondwana in late Paleozoic time (e.g., Ramezani and Tucker, 2003). Permian–Quaternary reconstructions of the Tethysides in the Middle East accordingly involve progressive break up and transfer of fragments of northern Gondwana and their accretion to the southern flank of Eurasia (e.g., Şengör and Natal'in, 1996). The most recent event of this type

is the mid-Tertiary rifting of Arabia away from Africa and its Miocene collision with Asia by closure of the Neotethys oceanic tract (e.g., Axen et al., 2001; McQuarrie et al., 2003), ultimately forming the folded belts of the Zagros Mountains to the south and the Alborz–Kopet Dagh ranges to the north (Fig. 1). The collisional suture between Arabia and Eurasia is along or perhaps somewhat north of the Zagros thrust zone, which juxtaposes folded and thrust strata of the Arabian platform against a stratigraphically and structurally more complex marginal assemblage referred to as the Sanandaj–Sirjan zone (Fig. 1).

Prior to the collision, plate convergence involved northward subduction of ~1300 km of Neotethyan oceanic lithosphere (e.g., McQuarrie et al., 2003), resulting in Andean-type magmatic arcs on the overriding continental plates that extend from the Balkan Peninsula to Afghanistan. The bulk of the Paleogene magmatic rocks in Iran are traditionally grouped into three belts: Alborz in the north, Urumieh–Dokhtar across central Iran, and Lut in the east (Fig. 1). Between the Alborz and Urumieh–Dokhtar belts is a large region of relatively low topography that includes the central-east Iranian microcontinent, as outlined by major faults (Takin, 1972).

The Saghand area is in the western part of the central-east Iranian microcontinent, ~100 km north-northeast of the axis of the Urumieh–Dokhtar arc (Fig. 1). The central-east Iranian microcontinent is subdivided into three

fault-bounded blocks, including (from east to west) the Lut, Tabas, and Yazd blocks (Fig. 1; e.g., Alavi, 1991). The boundary zone between the Tabas and Yazd blocks, the Kashmar–Kerman tectonic zone of Ramezani and Tucker (2003), forms a 50–100-km-wide, 600-km-long concave-east belt (Fig. 1) that exposes stratigraphically and structurally deep crustal levels (Cambrian stratified rocks, various crystalline units) that contrast with predominantly unmetamorphosed Mesozoic and younger rocks exposed elsewhere in the two blocks.

GEOLOGY OF THE SAGHAND REGION

Previous investigations in the Saghand area have included systematic mapping at scales of 1:100,000 to 1:500,000 (Valeh and Haghipour, 1970; Haghipour, 1977a, 1977b; Haghipour et al., 1977), and the detailed U-Pb zircon study of magmatic rocks in the area (Ramezani and Tucker, 2003). The area is crossed by two strike-slip faults of unknown age and net slip, the Posht-e-Badam and Chapedony faults (Fig. 2). Ramezani and Tucker (2003) subdivided the area into three lithotectonic domains, including an eastern, central, and western domain, based on lithostratigraphic and age characteristics. The eastern and central domains are juxtaposed along the Posht-e-Badam fault. The central domain is faulted over the western domain along the Neybaz and Chatak faults, which dip shallowly to

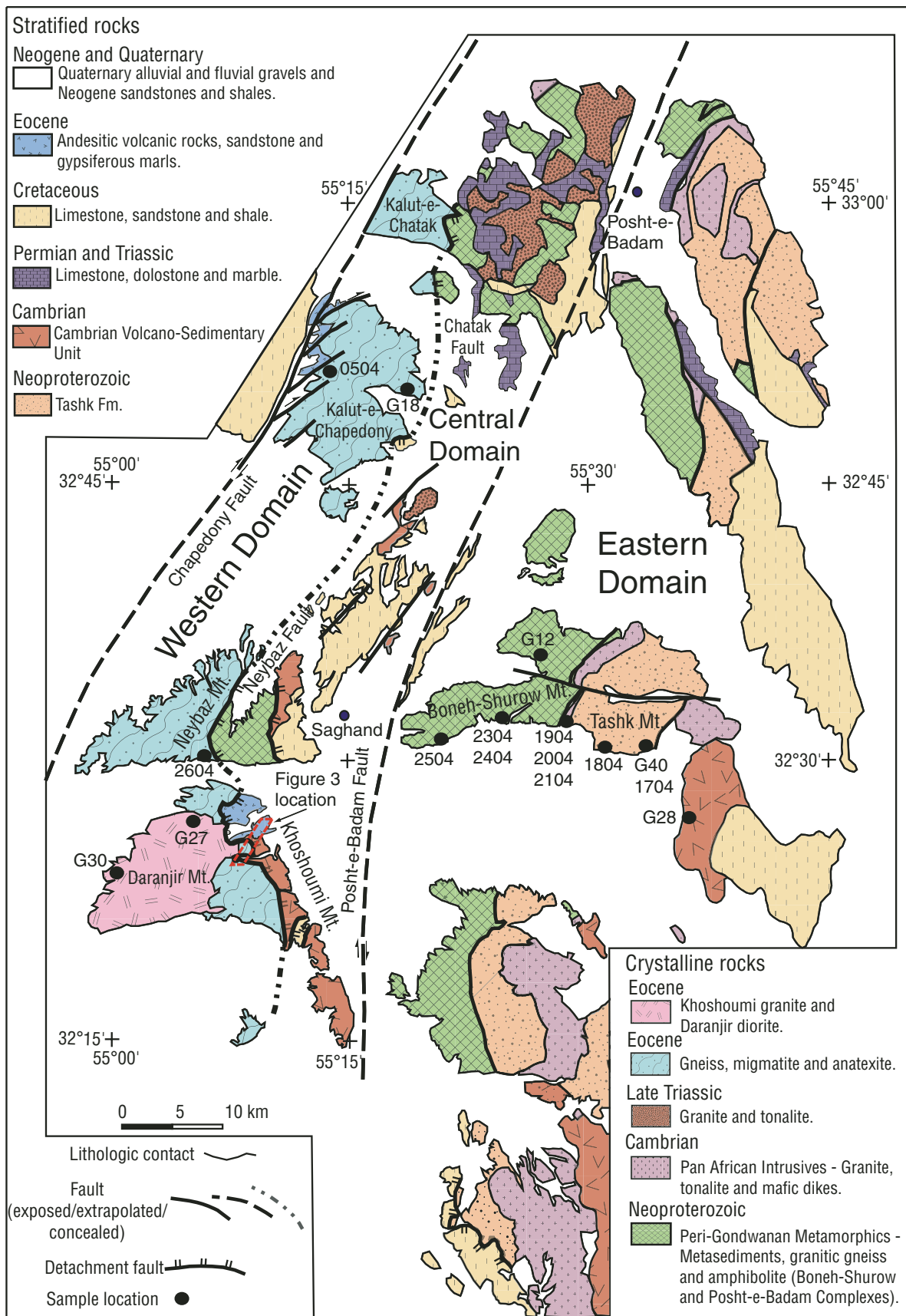


Figure 2. Geologic map of the Saghand area (modified from Ramezani and Tucker, 2003).

moderately east or northeast, and are not overlapped by any pre-Neogene strata. Although the contact between central and western domains is mainly exposed in two semicontinuous bands, it appears that a single low-angle fault system (the Neybaz-Chatak fault) juxtaposes the two domains over an along-strike distance of ~90 km (Fig. 2).

Bedrock exposures in the central and eastern domains constitute (1) stratified rocks that range in age from Ediacaran–Cambrian to Neogene (Fig. 2, upper left legend); (2) crystalline metamorphic complexes that include steeply foliated medium-grade felsic gneisses, schists, amphibolites, and marble, known as the Boneh-Shurow (eastern domain) and Posht-e-Badam (central domain) complexes; and (3) magmatic intrusive and subextrusive rocks of Early Cambrian (eastern domain) and Late Triassic (central domain) age (Fig. 2, lower right legend). The western domain is dominated by Eocene deep-seated metamorphic rocks and magmatic intrusions (Fig. 2, see also units defined in the lower right legend). The rock units relevant to this study are described in more detail below; stated age data in this section are those of Ramezani and Tucker (2003).

Stratified Rocks

The oldest stratified rocks include a thick succession of Ediacaran–Early Cambrian weakly metamorphosed graywackes, volcanoclastic rocks, and basaltic lavas, collectively referred to as the Tashk Formation. The formation contains detrital zircons as young as 627 Ma and was intruded by 533 Ma granitoid plutons. The Tashk Formation is overlain by the Cambrian volcano-sedimentary unit of Ramezani and Tucker (2003). These units are overlain in angular unconformity by Permian and Triassic shallow-marine carbonates.

Terrigenous and carbonaceous rocks of mid-Cretaceous age containing Aptian to Cenomanian fossils (e.g., *Orbitolina*) lie in angular unconformity on older Cambrian–Triassic units (Haghipour et al., 1977). Although the pre-Cretaceous hiatus spans ~100–400 m.y. within the Kashmar-Kerman tectonic zone, in the interior of the Yazd and Tabas blocks strongly folded marine strata as young as Middle Jurassic are in angular unconformity beneath the mid-Cretaceous strata (Haghipour et al., 1977). The stratigraphic record thus indicates that significant crustal shortening occurred within the central Iranian structural blocks between Middle Jurassic and mid-Cretaceous time and was concomitant with substantial erosion, particularly within the Kashmar-Kerman tectonic zone.

Volcanic rocks and associated sedimentary strata of Eocene age are widespread within

the central-east Iranian microcontinent and throughout Iran (Fig. 1), but are restricted to two relatively small areas in the Saghand region (Haghipour et al., 1977), one along the northwest flank of Kalut-e-Chapedony and another along the northeast side of Khoshoumi Mountain (Fig. 2). In the latter location, Haghipour et al. (1977) reported nummulitic marls indicating marine deposition, at least in part. As elaborated below, our observations of a steeply dipping section of these strata in excess of 1000 m thick suggest primarily nonmarine deposition in a rapidly subsiding basin, but confirm the Eocene age assignment of Haghipour et al. (1977).

The Eocene strata are overlain in angular unconformity by poorly consolidated evaporitic sandstones and mudstones that are probably Miocene or Pliocene (Haghipour et al., 1977). Near Saghand, these strata are at least several hundred meters thick and display a complex pattern of faulting and folding that suggests significant contractile deformation.

Crystalline Rocks

Within each of the five ranges that compose the eastern domain, the first-order structural pattern is that of an east-tilted crustal section, with Cretaceous strata exposed in the eastern portions of the ranges, east-dipping stratified rocks of the Tashk Formation and Cambrian volcano-sedimentary unit occupying the central portions, and deep-seated crystalline rocks of the Boneh-Shurow complex cropping out in the west (Fig. 2). The primary contact between the stratified rocks and subjacent crystalline rocks in both the central and eastern domains is a moderately to steeply east-dipping ductile shear zone. Plutonism and metamorphism in the Boneh-Shurow complex occurred ca. 545 Ma. Emplacement of granitoid plutons and intermediate to felsic volcanism associated with the Cambrian volcano-sedimentary unit occurred over a narrow temporal window of 533–525 Ma.

The western domain is composed almost entirely of high-grade gneissic rocks that form the Chapedony complex. This complex was long considered the oldest of the Precambrian units in the Saghand region, on the basis of its high metamorphic grade (Stöcklin, 1968; Haghipour et al., 1977), but U-Pb zircon dating demonstrates a middle Eocene intrusive age for the oldest components of these gneisses. Zircons from both synkinematic gneiss and migmatitic leucosomes derived from them have previously yielded concordia lower intercept ages of ca. 46 Ma (Ramezani and Tucker, 2003). The majority of the Chapedony complex is composed of gneiss, with lesser amounts of migmatite, anatectite, schist, marble, and calc-

silicate rock. The gneisses are locally amphibolitic but are predominantly medium to coarse biotite-feldspar-plagioclase-quartz gneiss with rare clinopyroxene and garnet. Medium to high metamorphic grade is indicated by large areas of migmatite and anatectite within the complex (Ramezani and Tucker, 2003).

Two postmetamorphic intrusions crop out at Daranjir Mountain (Fig. 2). The Daranjir diorite (U-Pb age 43.4 ± 0.2 Ma) is apparently the older of the intrusions. The Khoshoumi granite (U-Pb age 44.3 ± 1.1 Ma) overlaps in age, but intrudes both the Daranjir diorite and gneisses of the Chapedony complex. These ages and crosscutting relationships thus constrain metamorphism of the Chapedony complex to have occurred between 49 and 44 Ma (Ramezani and Tucker, 2003).

STRUCTURAL AND STRATIGRAPHIC OBSERVATIONS OF THE NEYBAZ-CHATAK DETACHMENT SYSTEM

Our new field observations include (1) geological mapping of an ~6-km-long transect across the detachment system along the northeast flank of Khoshoumi Mountain (western domain), where all of the primary extensional tectonic elements are exposed; (2) mesoscopic structural data from mylonitic gneisses at Khoshoumi Mountain, Neybaz Mountain, and Kalut-e-Chapedony; (3) structural microanalysis of lower plate mylonitic gneisses; (4) photographic documentation of key structural and stratigraphic relationships in the area; and (5) structural reconnaissance of the western end of Boneh-Shurow Mountain using high-resolution satellite imagery.

Neybaz-Chatak Detachment Fault and Hanging-Wall Splays

The Neybaz-Chatak detachment system without exception places lower temperature rock assemblages on top of higher. On the east side of Khoshoumi Mountain, the detachment places Eocene supradetachment basin deposits and the weakly metamorphosed to unmetamorphosed Cambrian volcano-sedimentary unit over mylonitic gneiss of the Chapedony complex (Fig. 2). At Neybaz Mountain and Kalut-e-Chatak it places medium-grade greenstones of the Posht-e-Badam complex over high-grade gneiss, and at the southeast tip of Kalut-e-Chapedony it places unmetamorphosed Cretaceous limestone over high-grade gneiss. Above the main contact with Chapedony complex gneisses along the eastern flanks of Neybaz Mountain and Khoshoumi Mountain, low- and high-angle splays juxtapose lower grade rocks on higher, or where both units are stratified, younger rocks on top of older.

Along the Khoshoumi Mountain transect, the detachment juxtaposes the strongly gouged and brecciated Cambrian volcano-sedimentary unit over mylonitic gneiss, and a hanging-wall normal fault juxtaposes Eocene sedimentary rocks against the Cambrian volcano-sedimentary unit (Fig. 3). The detachment contact in general dips gently to the north, but is strongly curvilinear, forming an east- to northeast-trending antiform-synform pair (Figs. 3 and 4A). In outcrop, the detachment varies from being a diffuse zone of gouge and breccia a few meters wide to a sharply defined plane (Fig. 5A). The gouge zones associated with the detachment and its hanging-wall splays are at least tens of meters thick (Fig. 5B) and exhibit phacoidal structure, with lozenge-shaped blocks of ~1–10 m in maximum dimension set in a matrix of gouge (Fig. 5C).

Immediately below exposures of the detachment, tabular zones of chlorite breccia were observed at Khoshoumi Mountain (Fig. 5A), Neybaz Mountain (Fig. 6A), and along the western flank of Kalut-e-Chapedony. At the latter locality the detachment places Cretaceous limestone on chlorite breccia of mylonitic gneiss, with brecciation affecting a structural thickness of mylonite (measured perpendicular to foliation) of ~100 m. Brecciation and chloritization become much less intense downward through the zone, which has a well-defined base (Fig. 5D).

Mylonites

As first observed by Haghipour et al. (1977), “huge parts” of the Chapedony complex are mylonitic. Mylonitization of augen gneiss and late-stage pegmatites within the gneiss is widespread on Khoshoumi Mountain, Neybaz Mountain (Figs. 6B, 6C), and at Kalut-e-Chapedony (Fig. 5E). The mylonites typically are composed of feldspar porphyroclasts in a matrix of biotite and fine-grained, recrystallized quartz and feldspar (Fig. 6D). Recrystallized quartz and feldspar grains average ~100 μm and ~25 μm in diameter, respectively. Quartz is typically recrystallized by subgrain rotation, while recrystallization of feldspar is primarily from bulging recrystallization (e.g., Passchier and Trouw, 2005). These textures, along with abundant myrmekite, suggest that mylonitization occurred in the upper part of the medium-grade conditions field (450–600 °C) of Passchier and Trouw (2005). Textures range from protomylonite to ultramylonite, often within single outcrops (Fig. 6B). Although lineation or foliation may be difficult to detect in some outcrops, the mylonites tend to be well-developed L-S tectonites with low to moderate dip and plunge, the lineation bisecting conjugate joints (Fig. 5E).

Foliation and lineation orientations were measured in three areas: on the south side of Neybaz Mountain, in the mapped transect on the east side of Khoshoumi Mountain (Fig. 3), and in the central part of Kalut-e-Chapedony (Fig. 2). In the latter two areas, measurements were distributed over an area of 1–2 km². The orientations at Kalut-e-Chapedony are distinctly different from those in the two areas to the south. At Kalut-e-Chapedony, foliation typically strikes roughly north-south and dips fairly gently to the west, with lineation plunging an average of 12°WSW (Fig. 7A). At Neybaz and Khoshoumi Mountains, attitudes are more scattered, but, on average, foliation dips north and lineation plunges 43°N (Fig. 7B).

Well-developed S-C texture is preserved in mylonitic orthogneiss along the southern flank of Neybaz Mountain, yielding top-to-the-north sense of shear (Fig. 6C). Oriented samples of eight other mylonites, five from Kalut-e-Chapedony and three from Khoshoumi Mountain, were slabbed and sectioned parallel to lineation and perpendicular to foliation to evaluate sense of shear. The Kalut-e-Chapedony samples yielded three top-to-the-west determinations and one top-to-the east (Fig. 7A). The samples from Khoshoumi Mountain yielded two top-to-the south determinations and one top-to-the north determination (Fig. 7B). The occurrence of oppositely directed shear sense indicators is common, if not ubiquitous, in mylonitic rocks (Hippertt and Tohver, 1999), and may suggest an important component of pure shear contraction normal to the flow direction (e.g., Lee et al., 1987).

Supradetachment and Postextensional Basinal Deposits and Structures

At least 1000 m of Tertiary nonmarine sandstone, siltstone, conglomerate, breccia, and volcanic rocks are exposed on the northeast flank of Khoshoumi Mountain (Fig. 4A). In the map transect (Fig. 3), these strata dip steeply southeastward, and are truncated along a moderately to steeply north dipping normal fault that places them on top of brecciated Cambrian strata. Tectonic lenses of Cretaceous conglomerate are locally present along the fault contact. The Tertiary strata are intruded by a dacite plug, which exhibits well-developed flow foliation and consists of an older phase to the west (Tev1 in Fig. 3) and a younger phase to the east (Tev2 in Fig. 3). The intrusive contact is subparallel to the flow foliation, and both dip steeply inward toward the dome in a radial pattern. Attitudes of bedding in the country rock appear to be deflected into parallelism with the margins of the plug as a result of emplacement (Fig. 3). Small outliers of the main intrusive are on the southwestern

side, one of which intrudes brecciated Cambrian volcano-sedimentary unit strata south of the normal fault that juxtaposes Cambrian and Tertiary rocks. Given the kilometer-scale offset along the normal fault and the lack of brecciation in the outlier within the Cambrian strata, we interpret these relations to indicate that intrusion occurred after faulting and brecciation of the Cambrian volcano-sedimentary unit. The steep inward dips of flow foliation around the dome further suggest that intrusion may have postdated most tilting of the Tertiary section, assuming that the plug intruded vertically.

The lower part of the Tertiary section southwest of the intrusive plug is primarily sandstone and siltstone, but has at least one rock avalanche deposit a few meters thick containing clasts of Cambrian volcanic rocks (Fig. 5F). We interpret these strata as a fault scarp facies developed in the early stages of detachment faulting, whereby the upper crust was fragmented into fault blocks, just prior to major rotation of hanging-wall strata and final ascent of mylonitic gneisses to the surface.

Along the northeast margin of Khoshoumi Mountain, a marked angular unconformity is observed between the steeply tilted Tertiary strata and overlying Neogene(?) nonmarine strata, which dip gently northeastward (Figs. 3 and 4A). The origin of tilting of the younger strata is not clear from relationships around Khoshoumi Mountain. However, in the extensive exposures of these deposits in low-relief badlands just east of Saghand (Haghipour et al., 1977), a large, open, gently west plunging anticline with gently to moderately dipping limbs is developed within these deposits. The anticline is cored by basement rocks of the Boneh Shurow complex, and is aligned with the long axis of the topographic ridge comprising Boneh-Shurow Mountain and Tashk Mountain (Figs. 2 and 4B). This relationship indicates that some or all of the topography of the region may be controlled by postextensional, approximately north-south tectonic shortening.

GEOCHRONOLOGY AND THERMOCHRONOLOGY

U-Pb Geochronology

We determined one additional U-Pb zircon age from mylonitic (augen) orthogneiss of the Chapedony complex at Neybaz Mountain (sample 2604, GSA Data Repository Table S1¹;

¹GSA Data Repository item 2007170, Tables S1–S5 and Appendices A–C, is available at <http://www.geosociety.org/pubs/ft2007.htm> or by request to editing@geosociety.org.

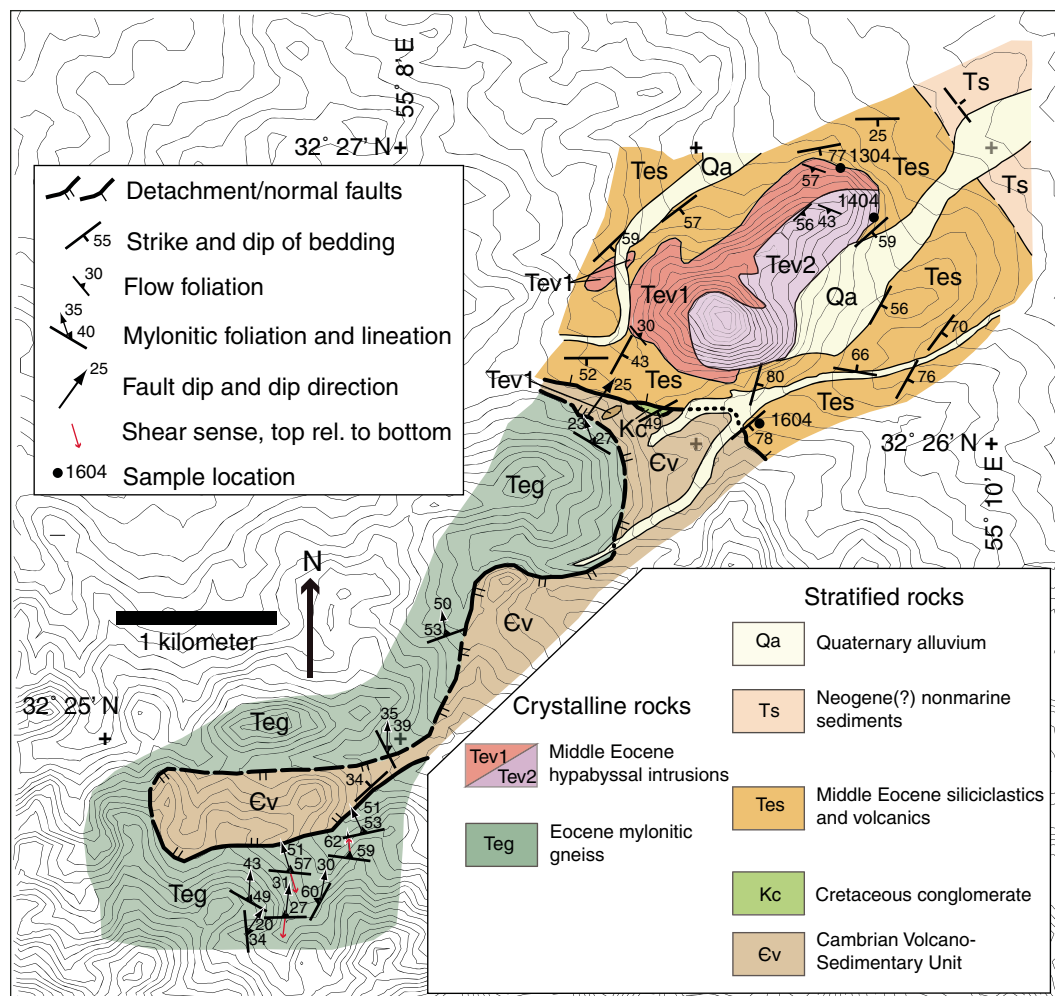


Figure 3. Geologic map of part of the east side of Khoushoumi Mountain showing $^{40}\text{Ar}/^{39}\text{Ar}$ sampling locations. See Figure 2 for location.

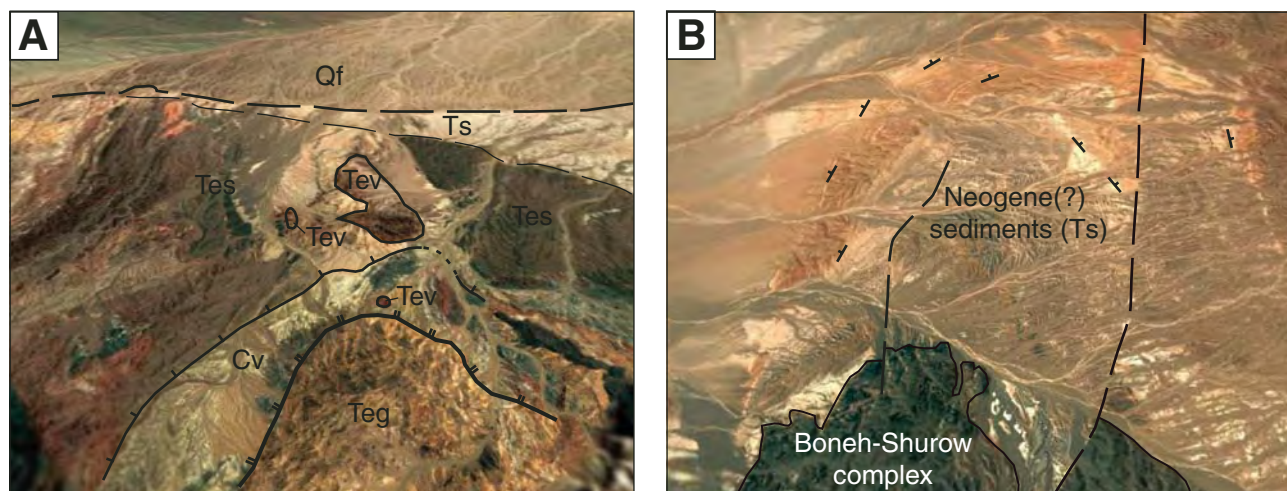


Figure 4. Oblique high-resolution satellite images. (A) View northeast along the eastern edge of Khoushoumi Mountain showing east-southeast-dipping Eocene supradetachment basin deposits (Tes) intruded by Eocene hypabyssal rocks (Tev), faulted over the Cambrian volcano-sedimentary unit (Cv) and Eocene gneiss (Teg). The Eocene sediments and volcanics are unconformably overlain by Neogene(?) sediments (Ts) and alluvial fan deposits (Qf). See Figure 3 for geologic map of this area. Width of view at center of image is 4.5 km. (B) View west of the western margin of Boneh-Shurow Mountain showing broad, approximately east-west-trending fold and opposing dips of Neogene(?) sediments. Width of view at center of image is 4.6 km. (Images from Google Earth, ©2006 Google™, ©2007 Europa Technologies, ©2007 Digital Globe, ©2007 TerraMetrics.)

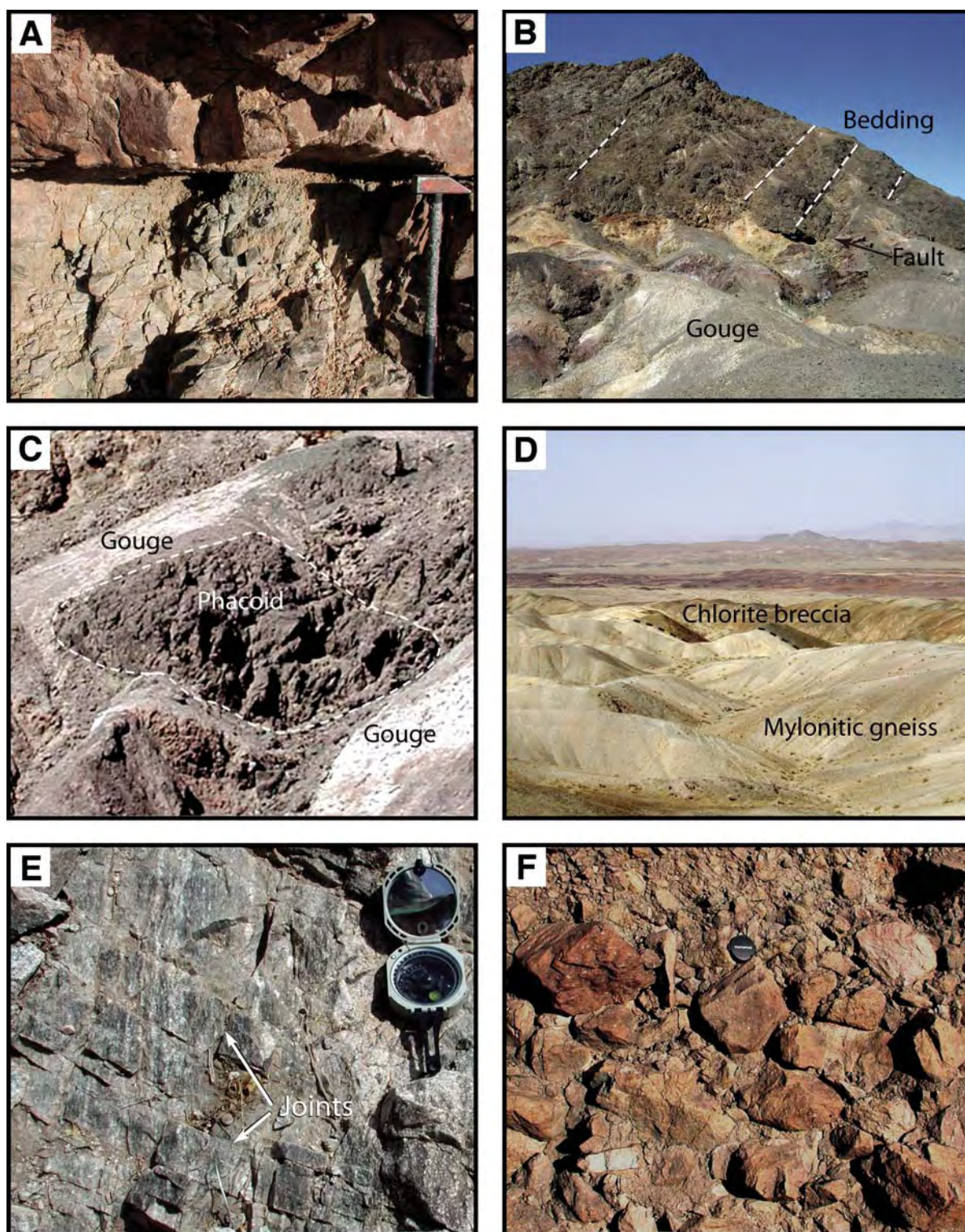


Figure 5. Field photographs of extensional features in the Saghand area. (A) View north-northeast of detachment fault emplacing Cambrian volcanic strata over chlorite breccia of mylonitic Chapedony gneiss, Khoshoumi Mountain (locality of fault plane attitude, Fig. 3). Hammer is 33 cm long. (B) View north of steeply west tilted Cretaceous limestone faulted over cataclastic Cambrian shale and volcanics exhibiting chaos structure. Width of view is ~200 m. (C) Close-up view of chaos structure showing phacoid (~3 m wide) surrounded by gouge. (D) View west showing base of chlorite breccia zone (dark band in middle ground), west side of Kalut-e-Chapedony. Light gray rocks in the foreground are mylonitic gneiss of the Chapedony complex. Width of view in foreground is ~200 m. (E) S70W lineation in mylonitic Chapedony gneiss, with foliation-normal conjugate joints, west side of Kalut-e-Chapedony. Width of view is 42 cm. (F) Monolithic scarp breccia of Cambrian volcanic rocks in Tertiary supradetachment basin, Khoshoumi Mountain. Width of view is 0.7 m.

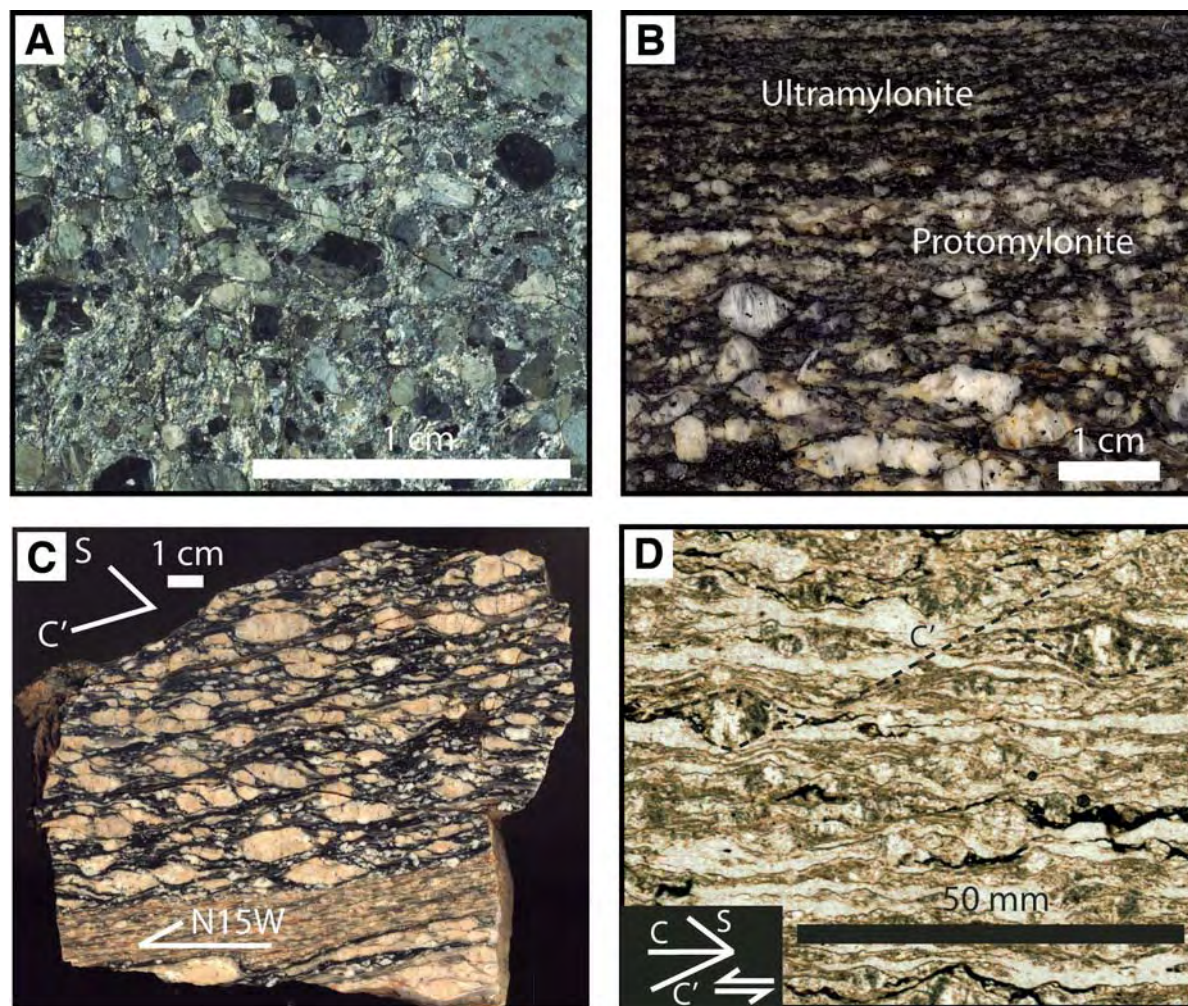


Figure 6. (A) Photomicrograph of chlorite breccia from Neybaz Mountain. (B) Polished slab of mylonitic Chapedony gneiss showing abrupt transition from ultramylonite to protomylonite, Kalut-e-Chapedony. (C) Polished slab of S-C mylonite with top to N15W shear sense, Neybaz Mountain. (D) Photomicrograph of mylonitic gneiss showing sigmoid porphyroclasts and extensional shear bands indicating top-to-the left shear sense, Kalut-e-Chapedony.

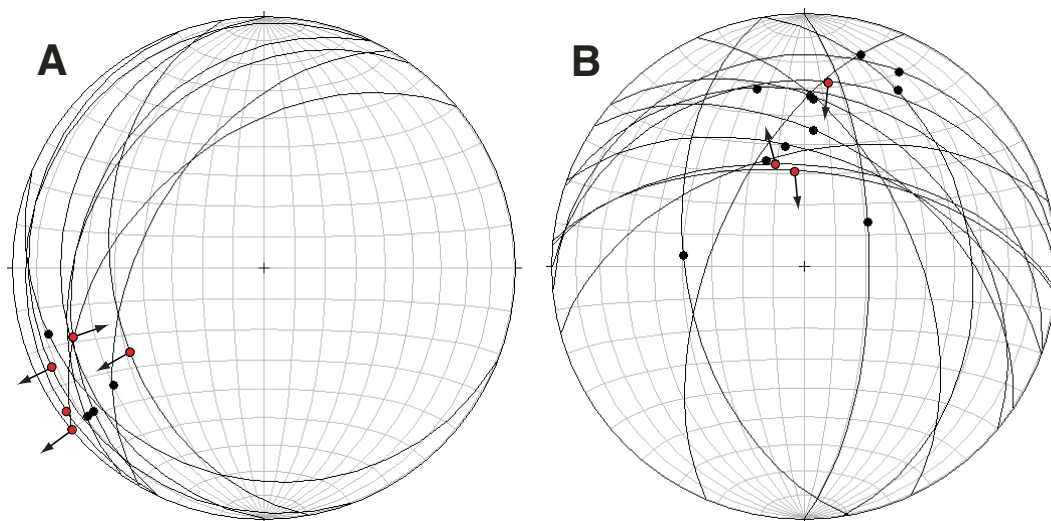


Figure 7. Lower hemisphere equal-area plots of mylonitic foliation and lineation orientations. (A) Kalut-e-Chapedony. (B) Khoushoumi Mountain. Red dots indicate oriented samples from which sense of shear directions were determined; arrows indicate relative motion of the top with respect to the bottom.

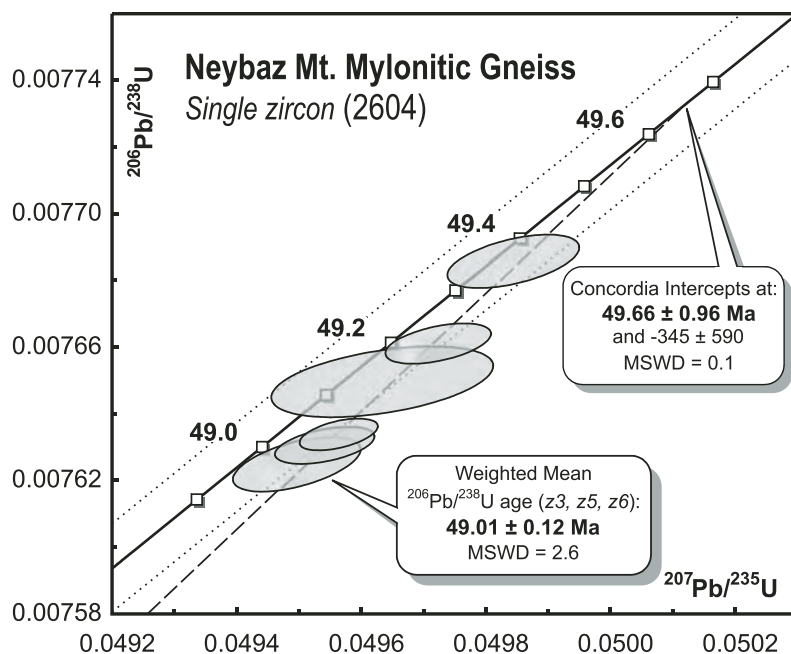


Figure 8. Concordia plot for zircons from sample 2604, a mylonitic gneiss from the southern edge of Neybaz Mountain (see Fig. 6C).

Figs. 2 and 6C). This sample consists of mica-rich bands enveloping K-feldspar and plagioclase porphyroclasts. Six single zircon grains were analyzed for Pb and U by the isotope dilution–thermal ionization mass spectrometry method at the Geochronology Laboratory at the Massachusetts Institute of Technology (Lehrmann et al., 2006; Schoene et al., 2006). The U–Pb isotopic dates and the associated uncertainties are calculated using the error propagation algorithm of Ludwig (1980) and are plotted with 2σ uncertainties on a conventional concordia plot (Fig. 8). The final uncertainties reported here incorporate both the internal (analytical) and external (systematic) sources of error. The latter includes the U–Pb tracer calibration error as well as the U decay constant errors of Jaffey et al. (1971). The incorporation of systematic errors in the calculated dates is necessary when results from different laboratories and/or different isotopic systems (e.g., U–Pb versus $^{40}\text{Ar}/^{39}\text{Ar}$) are compared (e.g., Schoene et al., 2006). Details of the U–Pb procedure are provided in Appendix A and Table S1 (see footnote 1).

Six U–Pb zircon analyses from sample 2604 produced an array of mutually distinctive $^{206}\text{Pb}/^{238}\text{U}$ dates ranging from 49.35 Ma to 48.97 Ma (Fig. 8). Regression of these data to a straight line yields an upper concordia intercept date of 49.66 ± 0.96 Ma (mean square of weighted deviate = 0.1). Alternatively, the three youngest analyses (z3, z5, and z6) overlap within error and yield a weighted mean $^{206}\text{Pb}/^{238}\text{U}$ date of

49.01 ± 0.12 Ma. The two calculated dates overlap within uncertainties and represent end-member estimates for the timing of zircon crystallization in the rock. These dates are consistent within uncertainties with a less precise 46.8 ± 2.5 Ma zircon date determined by Ramezani and Tucker (2003) from a nearby gneiss sample. Similarly, our measured ages can be interpreted as the timing of peak metamorphic and/or anatectic zircon crystallization in the Chapedony complex.

$^{40}\text{Ar}/^{39}\text{Ar}$ Geochronology

The ages of three samples from the Khoshoumi Mountain map transect were determined by $^{40}\text{Ar}/^{39}\text{Ar}$ geochronology techniques using a CO_2 laser and automated extraction line at the Berkeley Geochronology Center using the Fish Canyon sanidine (28.02 Ma; Renne et al., 1998) as a neutron flux monitor (Figs. 3 and 9; Table S2).

Sample 1604 was collected from a layer of biotite-rich volcanic ash within sediments from the hanging wall of the detachment. Samples 1304 and 1404 were collected from the dacite plug that intrudes the sediments (Fig. 3). Biotite from the ash has an $^{40}\text{Ar}/^{39}\text{Ar}$ inverse isochron age of 41.2 ± 2.4 Ma. Plagioclase from sample 1304 has an inverse isochron age of 42.0 ± 1.8 Ma, which is indistinguishable (within uncertainties) from an alkali feldspar age of 40.5 ± 2.5 Ma from sample 1404. Considering that the ash is near the top of the exposed section

and assuming that the dacite plug postdates both faulting and tilting, these ages suggest that faulting and tilting occurred between 39 and 43 Ma.

In addition, $^{40}\text{Ar}/^{39}\text{Ar}$ biotite ages were determined for six samples from a transect along Boneh-Shurow and Tashk Mountains (Fig. 2; Table S3). These ages represent the time since the samples cooled below the Ar closure temperature in biotite, which is ~ 300 – 350 °C under conditions of rapid cooling (≥ 10 °C/m.y.) (Harrison et al., 1985). The $^{40}\text{Ar}/^{39}\text{Ar}$ biotite ages were determined at the Nevada Isotope Geochronology Lab and are discussed in a following section. Details of the $^{40}\text{Ar}/^{39}\text{Ar}$ procedure are provided in Appendix B (see footnote 1).

(U–Th)/He Thermochronology

The (U–Th)/He ages were determined on apatite and zircon from Chapedony complex gneiss and postmetamorphic plutons as well as from Ediacaran–Cambrian rocks in the tilted crustal section of the eastern domain. These ages represent the time since the samples cooled below the He closure temperatures of apatite and zircon, which are ~ 70 °C and 190 °C, respectively (Wolf et al., 1996; Reiners et al., 2002). Apatite grains were placed in Pt tubes and heated with a Nd-YAG laser at the California Institute of Technology to extract helium, which was then analyzed by mass spectrometry (House et al., 2000). The grains were subsequently dissolved in nitric acid and analyzed with inductively coupled plasma mass spectroscopy to determine U and Th concentrations. Zircon (U–Th)/He ages were determined using a similar procedure but utilizing a flux of lithium metaborate to facilitate the dissolution of zircon in nitric acid (Tagami et al., 2003). Details of the (U–Th)/He procedure are provided in Appendix C.

Western Domain

The (U–Th)/He ages were determined from gneisses at Kalut-e-Chapedony and postmetamorphic plutons at Daranjir Mountain (Table S4; Fig. 2). Zircons from 0504, a sample of Chapedony gneiss, have an average (U–Th)/He age of 43.0 ± 7.8 (2σ) Ma; apatites from this sample have an age of 20.3 ± 5.8 Ma. G18, another sample of Chapedony gneiss, has a zircon (U–Th)/He age of 48.8 ± 15.6 Ma.

Zircons from samples G27 (Khoshoumi granite) and G30 (Daranjir diorite) yield (U–Th)/He ages of 40.5 ± 5.8 Ma and 40.6 ± 5.2 Ma, respectively. Apatites from these two samples have (U–Th)/He ages of 22.8 ± 3.3 and 15.4 ± 8.4 Ma, respectively.

These results suggest that both the gneisses of the Chapedony complex and the unmetamorphosed plutons cooled through the zircon

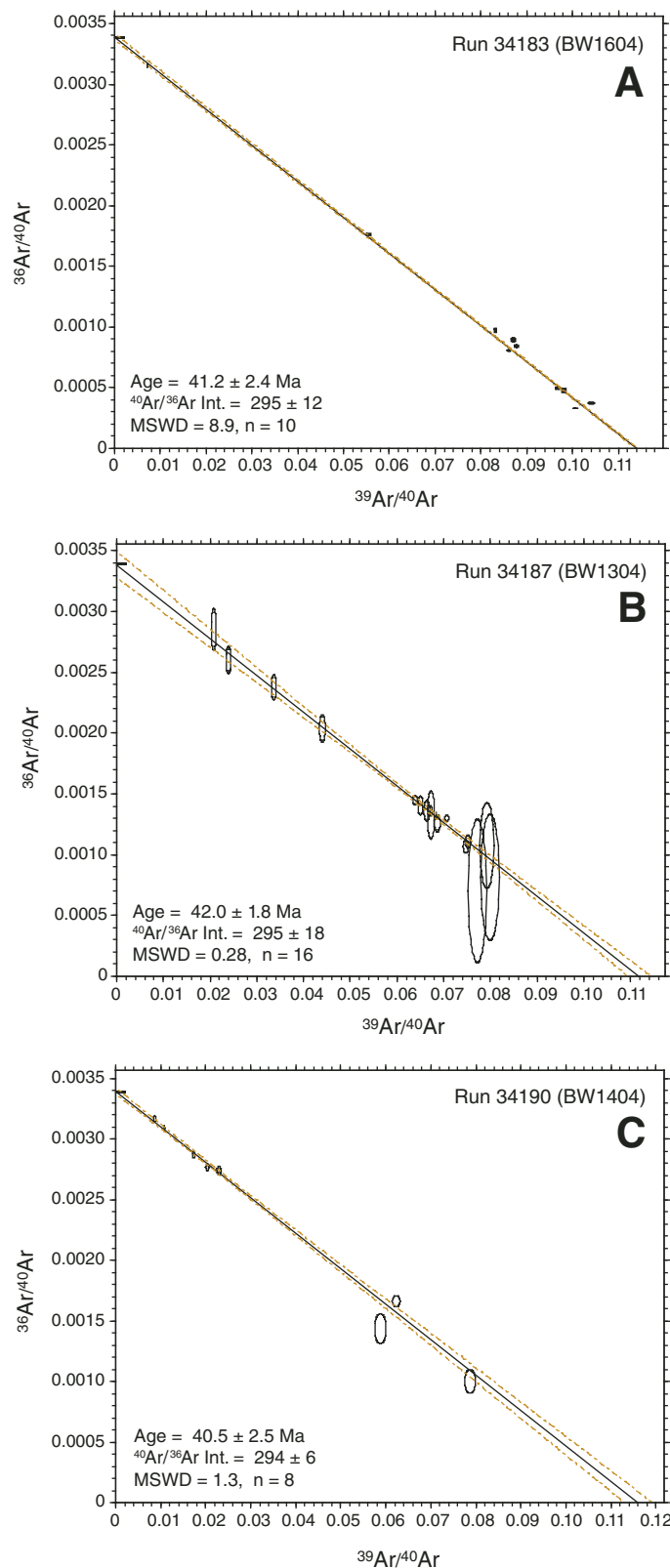


Figure 9. $^{40}\text{Ar}/^{39}\text{Ar}$ inverse isochron diagrams. All uncertainties are given at 95% confidence level. Int.—intercept. (A) 1604 biotite single grain total fusion analyses. The isochron exhibits excess scatter and the age uncertainty is expanded by $t^*\text{sqrt}$ (mean square of weighted deviates, MSWD). (B) 1304 plagioclase step heating of two multigrain aliquots. (C) 1404 alkali feldspar single grain total fusion analyses.

He partial retention zone during middle Eocene core complex formation. The overlap, within error, of U-Pb and zircon (U-Th)/He ages from the gneisses suggests rapid middle Eocene cooling. Subsequent cooling to $\sim 70^\circ\text{C}$ by ca. 20 Ma occurred at a much lower rate.

Eastern Domain

The presence of an east-tilted crustal section with >10 km of structural relief immediately east of the core complexes raises the issue of whether the crustal section was generated by flexural isostasy accompanying Eocene extension along a west-dipping detachment system, analogous to a number of examples in the North American Cordillera (Wernicke and Axen, 1988). In the Cordilleran examples, the tilting of crustal sections in the footwalls of major normal faults usually occurs rapidly, effectively quenching the thermal structure that existed within the crustal section just prior to unroofing (e.g., Fitzgerald et al., 1991; Foster et al., 1993; Reiners et al., 2000; Stockli, 2005). If the crustal section of the eastern domain was formed by Eocene extension, an east-west horizontal transect of cooling ages across the domain would be expected to yield progressively younger ages toward the west, reaching an Eocene minimum.

An ~ 20 -km-long horizontal depth profile along Boneh-Shurow and Tashk Mountains, from the unmetamorphosed Cambrian volcano-sedimentary unit near the top of the crustal section in the east to crystalline rocks at significant structural depth within the Boneh-Shurow complex to the west (Fig. 2), was sampled for (U-Th)/He and $^{40}\text{Ar}/^{39}\text{Ar}$ dating to determine the age of tilting. The (U-Th)/He apatite and zircon ages determined from this profile are primarily from detrital grains in sedimentary or metasedimentary rocks, and generally display a significant amount of scatter but do not vary systematically with structural position. Mean zircon (U-Th)/He ages range from 100 to 134 Ma and overlap (using 2σ errors) between 116 and 125 Ma. Mean apatite ages range from 17 to 20 Ma (Table S5; see footnote 1). In contrast, $^{40}\text{Ar}/^{39}\text{Ar}$ ages determined on metamorphic biotite from six of the samples exhibit variation with position. The $^{40}\text{Ar}/^{39}\text{Ar}$ biotite ages vary from 150–160 Ma in structurally deeper parts of the section to 218–295 Ma in the upper part. As is apparent from a plot of age versus structural position (Fig. 10A), the data indicate Late Jurassic tilting of the crustal section, followed by relatively uniform cooling of the entire section below $\sim 190^\circ\text{C}$ in mid-Cretaceous time, and cooling of at least the westernmost half of the section below $\sim 70^\circ\text{C}$ in early Miocene time. Late Jurassic tilting may also account for the ca. 150 Ma lower intercept ages of zircons from the Boneh-Shurow complex

(Fig. 10B), because decompression accompanying rapid exhumation of these structurally deep rocks may have cracked the zircons and facilitated Pb loss along microfractures.

DISCUSSION AND CONCLUSIONS

The region of Eocene gneisses in the Saghand area clearly contains all of the major tectonic elements known from metamorphic core complexes in the North American Cordillera. Each of the four ranges in the western domain contains a brittle fault placing various upper crustal assemblages on deep-seated gneisses, which is a signature observation along the 2000-km-long belt of core complexes in North America (e.g., Davis et al., 1980; Coney, 1980; Armstrong, 1982). The structural style of younger over older, moderate- to low-angle faults observed in central Iran is ubiquitous in the hanging-wall structure of Cordilleran detachments. A distinctive structural style of lozenge-shaped fault blocks bounded by gouge and breccia, termed chaos structure, has been described from a number of Cordilleran examples (Noble, 1941; Wernicke and Burchfiel, 1982; Wright and Troxel, 1984). Mylonitic gneisses are also ubiquitous in the footwalls of Cordilleran examples (e.g., Davis and Coney, 1979; Davis, 1980; Davis and Lister, 1988). In particular, where the footwalls of the Cordilleran examples are primarily granitic, as in the Sonoran Desert region, the development of L-S tectonite overprinted by chloritic brecciation (e.g., Reynolds, 1985; Spencer and Welty, 1986) bears strong similarity to the central Iran complexes. The development of thick deposits of primarily nonmarine sedimentary and volcanic successions containing rock avalanche breccias, steeply tilted and juxtaposed on structurally lower rocks, referred to as supradetachment basins (e.g., Friedmann et al., 1994), are well described from most Cordilleran examples.

The topographic expression of the mountain ranges bearing the Chapedony complex has been given the special term *kalut* in the local Farsi dialect, which signifies a tendency toward having a broad, flat upland area, in contrast to the relatively narrow, cusped ridge lines characteristic of surrounding ranges (Ramezani and Tucker, 2003). This pattern is similar to that of Cordilleran metamorphic core complexes, especially in the southwestern United States, where domes of variably mylonitic gneisses in the footwalls of extensional detachments are expressed by a domiform topography, or turtleback (e.g., Wright et al., 1974; Coney, 1980).

In addition to these common features, we further note that the tectonic setting of the Cordilleran examples is that of a continental or Andean-type magmatic arc (Coney, 1980; Armstrong,

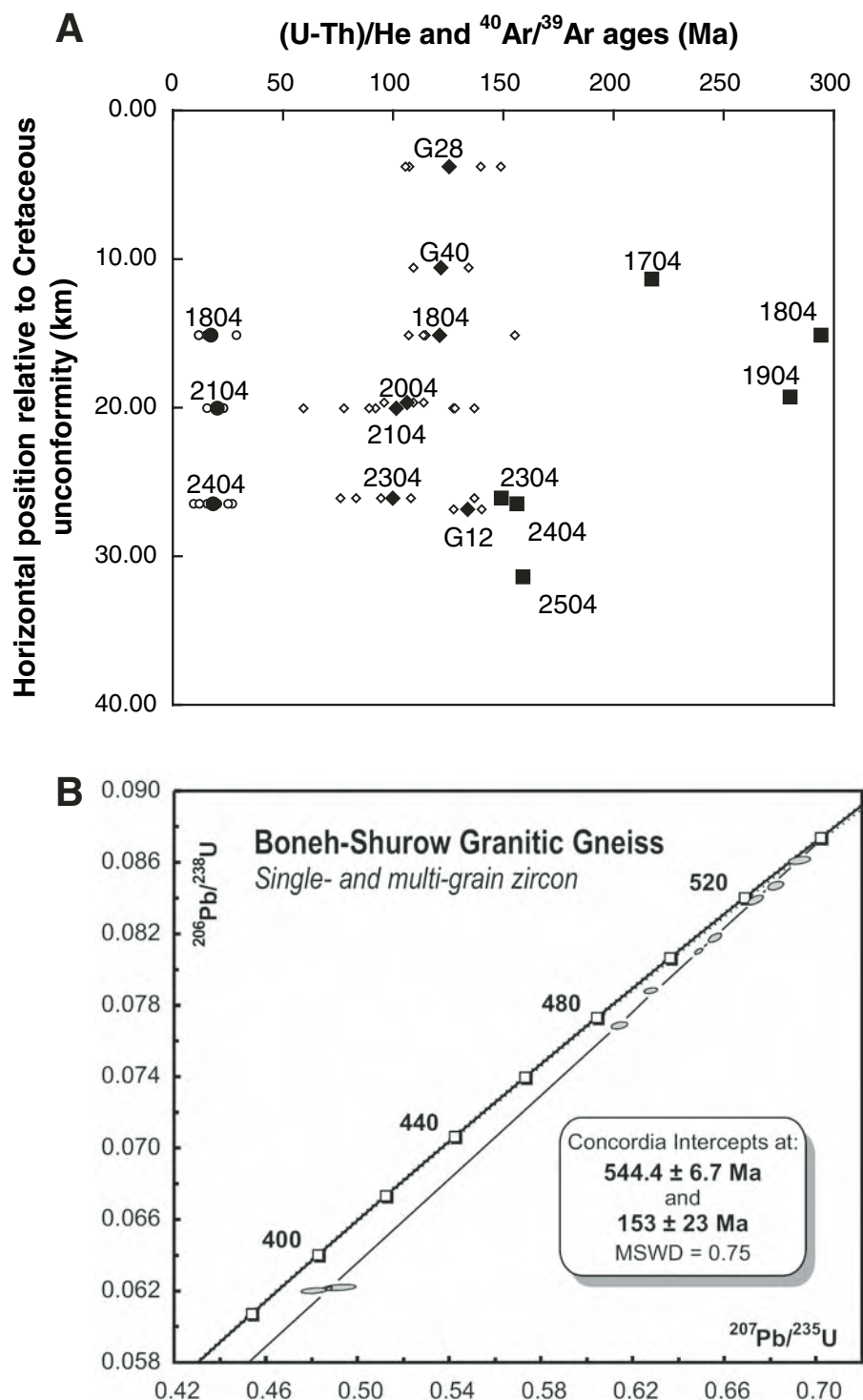


Figure 10. Thermochronologic data from the eastern domain. (A) (U-Th)/He apatite (circles) and zircon (diamonds) ages, along with $^{40}\text{Ar}/^{39}\text{Ar}$ biotite ages (squares) from eastern domain samples, plotted as a function of horizontal position within the east-tilted crustal section. For (U-Th)/He data, individual replicates are shown with open symbols, and mean ages are shown with filled symbols. Sample positions were determined by projection onto the direction N60W. (B) U-Pb concordia diagram for zircons from the Boneh-Shurow complex (for analytical details see Ramezani and Tucker, 2003). The upper intercept age is interpreted as the crystallization age of the protoliths, while the lower intercept age may reflect Pb loss resulting from rapid uplift. MSWD—mean square of weighted deviates.

1982; Armstrong and Ward, 1991). The middle Eocene time frame for the development of the Saghand area core complexes (see below) coincides with peak production of arc magmas in the Urumieh-Dokhtar, Alborz, Lut, and related magmatic arcs of central Iran. The protoliths of mylonitic plutons, the undeformed plutons of the Daranjir Mountain area, and volcanic strata within the supradetachment basin are all contemporaneous with the mid-Tertiary magmatic arc system of central Iran and are broadly synchronous with development of extension in the backarc region.

Timing of Extension

A summary of known (solid lines) and inferred (dashed lines) superposition relationships and relevant geochronologic data for the Khoshoumi Mountain transect is illustrated in Figure 11. Peak metamorphism (migmatization) and mylonitization of the Chapedony complex occurred between 44 and 49 Ma, based on

the oldest U-Pb zircon ages from Chapedony complex gneiss and the late-stage plutons at Daranjir Mountain. The $^{40}\text{Ar}/^{39}\text{Ar}$ age determinations indicate that as late as 41 Ma, a supra-detachment basin had formed in the hanging wall of the detachment. Not long after this time, the basin fill was steeply tilted and intruded by the dacite plug, which yields the same age, within uncertainties, as the biotite tuff within the basin. Given uncertainties of ± 2 m.y. on both ages, the maximum time available for post-tuff sedimentation, tilting, and final motion on the detachment and its hanging wall splays is 4 m.y. The age data therefore imply that mylonitization of extant igneous rock occurred between 49 and 44 Ma, and movement on the Neybaz-Chatak fault and supradetachment basin development was completed no later than 41 ± 2 Ma.

Kinematics of Extension

Data from the Saghand area are not sufficient to define the magnitude and direction of

extension that led to exhumation of the core complexes. The complete lithological mismatch between the hanging wall and footwall of the Neybaz-Chatak detachment system suggests an amount of extension that is at least as wide as the complexes, i.e., 30 km. Assuming that extension of this magnitude occurred over, at most, 4 m.y., as outlined above, we obtain a minimum average horizontal extension rate of ~ 8 mm/yr. The 4 m.y. time scale is quite similar to that observed for similar geochronologic data on Cordilleran examples (e.g., Holm and Dokka, 1993; Niemi et al., 2001; Walker et al., 1990; Wells et al., 2000; Gans and Bohrer, 1998), and the ~ 8 mm/yr rate is similar to those measured in both the Cordillera and the Aegean region (e.g., Kumerics et al., 2005; Ring et al., 2003).

In Cordilleran examples, the extension direction is usually indicated by three major criteria, independent of piercing points that might be observed between hanging wall and footwall. These include (1) development of extensive areas of extension-parallel mylonitization (e.g., Rehrig and Reynolds, 1980; Davis, 1980); (2) development of extension-parallel antiforms and synforms in the detachment surface at a variety of scales (e.g., John, 1987; Spencer and Reynolds, 1989); and (3) tilt direction of hanging-wall fault blocks including supradetachment basin deposits, such that the tilt direction is opposite to the transport direction on the detachment fault (e.g., Davis et al., 1980; Shackelford, 1980). A fourth, perhaps less robust, consideration is that in the Cordilleran examples, belts of core complex mountain ranges tend to be elongate perpendicular to the regional extension direction, for example, as in the lower Colorado River trough region of the Sonoran Desert (Spencer and Reynolds, 1989).

The orthogonality in the trend of lineations between Kalut-e-Chapedony and Khoshoumi Mountain and the lack of clear-cut asymmetry in shear direction make it difficult to apply the first criterion. Given the observation of significant post-Eocene deformation in the area, it is possible that the orthogonality of lineation trend is, at least in part, the result of vertical-axis rotations of the range blocks. In a paleomagnetic study of Cretaceous limestones just north of Saghand, Soffel et al. (1996) concluded that the tilt-corrected paleomagnetic pole for these strata is concordant with a modest number of other Cretaceous directions in the central-east Iranian microcontinent. We interpret these data to preclude major ($>30^\circ$) differential rotation of the Neybaz Mountain–Khoshoumi Mountain area with respect to the remainder of the central-east Iranian microcontinent. Furthermore, the continuity and general eastward dip of the Neybaz-Chatak fault along its entire length argue against

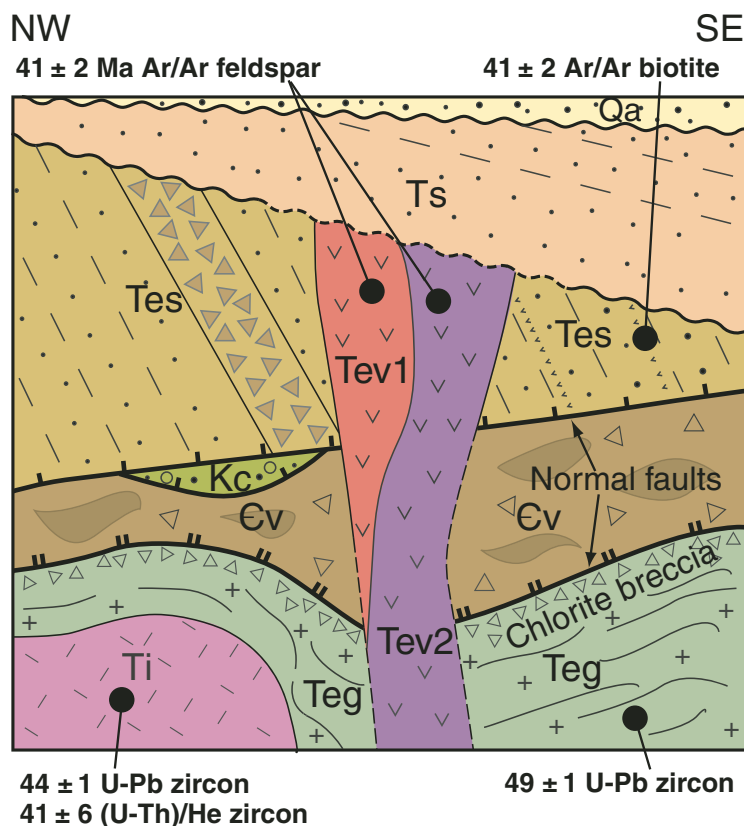


Figure 11. Summary of superposition relationships and $^{40}\text{Ar}/^{39}\text{Ar}$ data for the Khoshoumi Mountain area (Figs. 2 and 3). Solid lines indicate mapped relationships, and dashed lines indicate inferred relationships discussed in text. Qa—Quaternary alluvium; Teg—Eocene mylonitic gneiss; Ts—Neogene(?) sediments; Tes—middle Eocene siliciclastics and volcanics; Tev1, Tev2—middle Eocene hypabyssal intrusions; Ti—Eocene postmetamorphic intrusions; Kc—Cretaceous conglomerate; Ev—Cambrian volcano sedimentary unit.

major postextensional dismemberment and vertical-axis rotation of the core complex belt, and so we do not favor postextensional vertical-axis rotation as an explanation for the differing trends in mylonitic lineation.

Despite the general occurrence of extension-parallel mylonites in many core complexes, it is not uncommon to observe more than one flow direction in footwall mylonites (e.g., MacCready et al., 1997). Although in some instances footwall mylonites may be interpreted as the downdip continuation of brittle simple shear on their overlying detachments (e.g., Wernicke, 1981; Lister et al., 1984), much of the mylonitic gneiss in Cordilleran and other examples is now regarded as the result of mid-crustal channel flows directed toward the area of maximum unroofing during extension (e.g., Wernicke, 1992; Brun et al., 1994; MacCready et al., 1997). Therefore, our preferred interpretation of the nearly orthogonal trends of the mylonitic lineations is that the Kalut-e-Chapedony mylonites represent eastward flow of middle crustal rocks toward the region of denudation early in the extension process, and the Khoshoumi Mountain and Neybaz Mountain mylonites, located along the southern margin of the extended region, record northward flow toward the same region.

The criteria of antiforms and synforms are also difficult to evaluate. Neybaz and Khoshoumi Mountains and Kalut-e-Chatak are elongate roughly east-west, but Kalut-e-Chapedony is slightly elongate north-south. On the whole, this would appear to suggest east-west extension, but the topographic pattern is in general not as regular as that for the best Cordilleran examples. Furthermore, given the evidence for postextensional folding in the area, the morphology of the core complex ranges could relate more to an episode of Neogene folding than to the episode of Eocene extension.

The hanging-wall tilt directions of the supradetachment basin deposits along the northeast flank of Khoshoumi Mountain are approximately east-southeast, implying west-northwest displacement on the detachment system. As with the other criteria, tilt direction in Cordilleran examples is not always opposite the direction of slip on the fault, and in several instances has been shown to be either in the same direction as slip (e.g., Wernicke, 1985), or significantly oblique to the extension direction (e.g., Hodges et al., 1989).

Although further work is clearly required to resolve the issue, the north-northeast trend of the belt of core complexes, the east-southeast tilt direction of the supradetachment basin at Khoshoumi Mountain, the approximately east-west elongation direction of three of the four core complex ranges, and the west-southwest trend

of mylonitic lineation at Kalut-e-Chapedony suggest an overall east-west extension direction, with transport on the detachment top to the west. We interpret the northward lineation direction at Khoshoumi and Neybaz Mountains to be the result of extension-normal flow of deep-crustal rocks from unextended areas in the south toward the region of maximum unroofing to the north.

Cretaceous and Miocene (U-Th)/He Cooling Ages

Although the eastern and western domains both yield Miocene apatite ages, the Cretaceous zircon cooling ages from the eastern domain contrast strongly with the Eocene zircon cooling ages from the western domain. The $^{40}\text{Ar}/^{39}\text{Ar}$ biotite ages and uniformity of (U-Th)/He apatite and zircon ages across the crustal section indicate that tilting and rapid cooling, perhaps due to contractional deformation in the region, occurred in the Late Jurassic. A regional angular unconformity separates Albian(?) to Cenomanian strata from Middle Jurassic and older rocks.

Miocene (U-Th)/He apatite ages obtained from both the western and eastern domains suggest a period of exhumation that postdates extension by ~20 m.y. Assuming a mid-Tertiary geothermal gradient of 30 °C/km, appropriate for continental arc terrain, and a mean surface temperature of 10 °C, a pre-Miocene depth of ~2000 m is indicated by these ages. We interpret these ages to reflect cooling related to approximately north-south shortening of the region, as suggested by the folding of Neogene strata near Saghand (Fig. 4B). The development of a major early Miocene east-west-trending fold raises the question of whether this deformation is related to the Arabia-Eurasia collision. According to the palinspastic and plate tectonic arguments presented by McQuarrie et al. (2003), 20 Ma is the earliest possible time of collision between Arabia and central Iran. If the age of initial collision is closer to 10 Ma, as preferred by McQuarrie et al. (2003), then the fold would represent shortening in an Andean-type setting and would suggest a precollisional transition from extension to compression in the overriding plate at some time between ca. 40 and 20 Ma, as suggested by Vincent et al. (2005) on the basis of stratigraphic data from Azerbaijan. Such a transition occurred there near the end of the Eocene, which they interpreted as supporting previous suggestions that the initial collision occurred ca. 40 Ma. Although data collected during this study only indirectly bear on this issue, the simple plate tectonic and palinspastic arguments indicate that at 40 Ma there was >1000 km of separation between central Iran and the Zagros Mountains. Clearly the details of how various Neo-Tethyan

continental fragments may have interacted with one another are at issue, but wholesale arrival of the Arabian subcontinent against contiguous, south Asian continental crust (i.e., the broadest possible definition of the initial collision of Arabia with Eurasia, as opposed to the collision of intra-Tethyan continental fragments) by 40 Ma is unlikely.

Regional Significance

In addition to the core complexes exposed near Saghand, core complexes have also been reported in northwest (Stockli et al., 2004) and northeast (Hassanzadeh et al., 2005) Iran (Fig. 1). Geologic maps (Thiele et al., 1967; Tillman et al., 1981) and satellite image reconnaissance strongly suggest the presence of a fourth Iranian core complex in southwest Iran near the town of Golpaygan (Fig. 1). Available thermochronologic data indicate that the Iranian core complexes may span a range in age from Late Cretaceous to early Miocene. Prior to these reports, there were no known regions of significant Tertiary extension within the Tethysides between the Bitlis suture in eastern Turkey and the western Himalayan syntaxis. The widespread occurrence of core complexes in Iran demonstrates that core complex development has affected every major segment of the Tethysides (Fig. 12; Table 1).

Formation of the Cretaceous–Cenozoic core complexes of the Alpine–Himalayan orogen is usually attributed to backarc extension associated with rapid subduction, or slab rollback, such as in the Tyrrhenian basin (e.g., Royden, 1993), or to large gradients in gravitational potential energy within the lithosphere resulting from localized crustal thickening (e.g., Dewey, 1988). The former has been invoked by some to account for the numerous core complexes of Spain, western Turkey, and the Tyrrhenian and Aegean Seas (e.g., Brunet et al., 2000; Buick, 1991; Dinter, 1998; Lonergan and White, 1997; Okay and Satir, 2000; Thomson et al., 1999), while others have suggested that the latter process is responsible for extensional structures in Spain, the Himalayas, and eastern China (Platt and Vissers, 1989; Burchfiel et al., 1992; Davis et al., 2002; respectively). Extension in the eastern Alps has been ascribed to a combination of gravitational collapse and tectonic escape (e.g., Ratschbacher et al., 1991a, 1991b). Extension in the Saghand region long predated any intracontinental shortening resulting from direct contact between Arabia and Eurasia, which argues against core complex formation as the result of thickened crust or the eastward extrusion of the central-east Iranian microcontinent (Fig. 1). The extension direction appears to be oblique, or perhaps subparallel, to

TABLE 1. ALPINE-HIMALAYAN METAMORPHIC CORE COMPLEXES

Number (Fig. 12)	Location/Name	Age	Extension direction	Reference
<u>Spain</u>				
1	Nevado-Filabrides	Late Oligocene–late Miocene	NW-SE	Platt and Vissers, 1989
2	Sierra Alhamilla	Late Oligocene–late Miocene	NNE-SSW	Platt and Vissers, 1989
3	Sierra de las Estancias	Late Oligocene–early Miocene	NNE-SSW	Platzman and Platt, 2004
<u>Algeria</u>				
4	Edough	Late Miocene	NW-SE	Caby et al., 2001
<u>Alps</u>				
5	Simplon	Oligocene–Miocene	NE-SW	Mancktelow and Pavlis, 1994; Wawrzyniec et al., 2001
6	Brenner	Early Oligocene–early Miocene	E-W	Axen et al., 1995; Wawrzyniec et al., 2001
7	Rechnitz	Oligocene–Miocene	E-W	Grassl et al., 2004; Ratschbacher et al., 1990
<u>Italy–Tyrrhenian Sea</u>				
8	Corsica	Late Oligocene–early Miocene	ENE-WSW	Brunet et al., 2000; Fournier et al., 1991
9	Alpi Apuane	Miocene	NE-SW	Carmignani and Roy, 1990; Carmignani et al., 1994
10	Monte Pisano	Pliocene	NE-SW	Brunet et al., 2000
11	Monticciano-Roccastrada	Pliocene	E-W	Brunet et al., 2000
12	Elba	Miocene	E-W	Brunet et al., 2000
13	Monte Romani	Miocene–Pliocene	ENE-WSW	Brunet et al., 2000
14	Uccellina	Miocene		Brunet et al., 2000
15	Monte Argentario	Miocene	ENE-WSW	Brunet et al., 2000
16	Gorgona	Miocene	NW-SE	Brunet et al., 2000
17	Giglio	Miocene	ENE-WSW	Jolivet et al., 1998
18	Calabrian	Middle Oligocene–middle Miocene	N-S	Platt and Compagnani, 1990; Thomson, 1994; Wallis et al., 1993
<u>Carpathians</u>				
19	Vepor	Cretaceous	NE-SW	Janak et al., 2001
20	Getic	Late Eocene–Oligocene	WSW-ENE	Fugenschuh and Schmid, 2005; Schmid et al., 1998
<u>Bulgaria/Northern Greece</u>				
21	Osogovo-Lisets	Middle Eocene–early Oligocene	NE-SW	Kounov et al., 2004
22	Rhodope	Miocene	NE-SW	Dinter et al., 1995; van Hinsbergen and Meulenkamp, 2006
<u>Greece/Aegean Sea</u>				
23	Thasos	Early–middle Miocene	NE-SW	Wawrzyniec and Krohe, 1998
24	Mykonos	Late Miocene	NE-SW	Lee and Lister, 1992
25	Naxos	Miocene	NNE-SSW	Lister et al., 1984
26	Ios	Miocene	NNE-SSW	Lister et al., 1984
27	Tinos	Miocene	NNE-SSW	Gautier and Brun, 1994; Ring et al., 2003
28	Andros	Miocene	NNE-SSW	Gautier and Brun, 1994
29	Evvia	Oligocene–early Miocene	ENE-WSW	Gautier and Brun, 1994
30	Ikaria	Late Miocene–Pliocene	NNE-SSW	Kumerics et al., 2005
31	South Aegean (Cretan)	Early-middle Miocene	N-S	Thomson et al., 1999; van Hinsbergen and Meulenkamp, 2006
<u>Turkey</u>				
32	Kazdag	Late Oligocene	NNW-SSE	Okay and Satir, 2000
33	Simav	Early-middle Miocene	NNE-SSW	Ring and Collins, 2005
34	Central Menderes	Miocene–present	N-S	Gessner et al., 2001
35	Nigde	Miocene–present	NE-SW	Whitney and Dilek, 1997
<u>Iran</u>				
36	Takab-Zanjan	Miocene	NW-SE	Stockli et al., 2004
37	Golpaygan			Thiele et al., 1967; Tillman et al., 1981
38	Saghand	Middle Eocene	E-W	This paper
39	Biarjmand	Cretaceous	NE-SW	Hassanzadeh et al., 2005
<u>Himalaya</u>				
40	Kongur Shan	Early Pliocene–present	E-W	Brunel et al., 1994
41	Nanga Parbat	Early Miocene	WSW-ENE	Argles and Edwards, 2002; Hubbard et al., 1995
42	N. Himalayan gneiss domes	Miocene	N-S	Burchfiel et al., 1992; Yin et al., 1999
43	Mabja Dome	Miocene	N-S	Lee et al., 2004
44	Kangmar Dome	Miocene	N-S	Chen et al., 1990; Lee et al., 2000
<u>Eastern China</u>				
45	Hohhot	Early Cretaceous	N-S	Davis et al., 2002
46	Liaonan	Early Cretaceous	NW-SE	Junlai et al., 2005

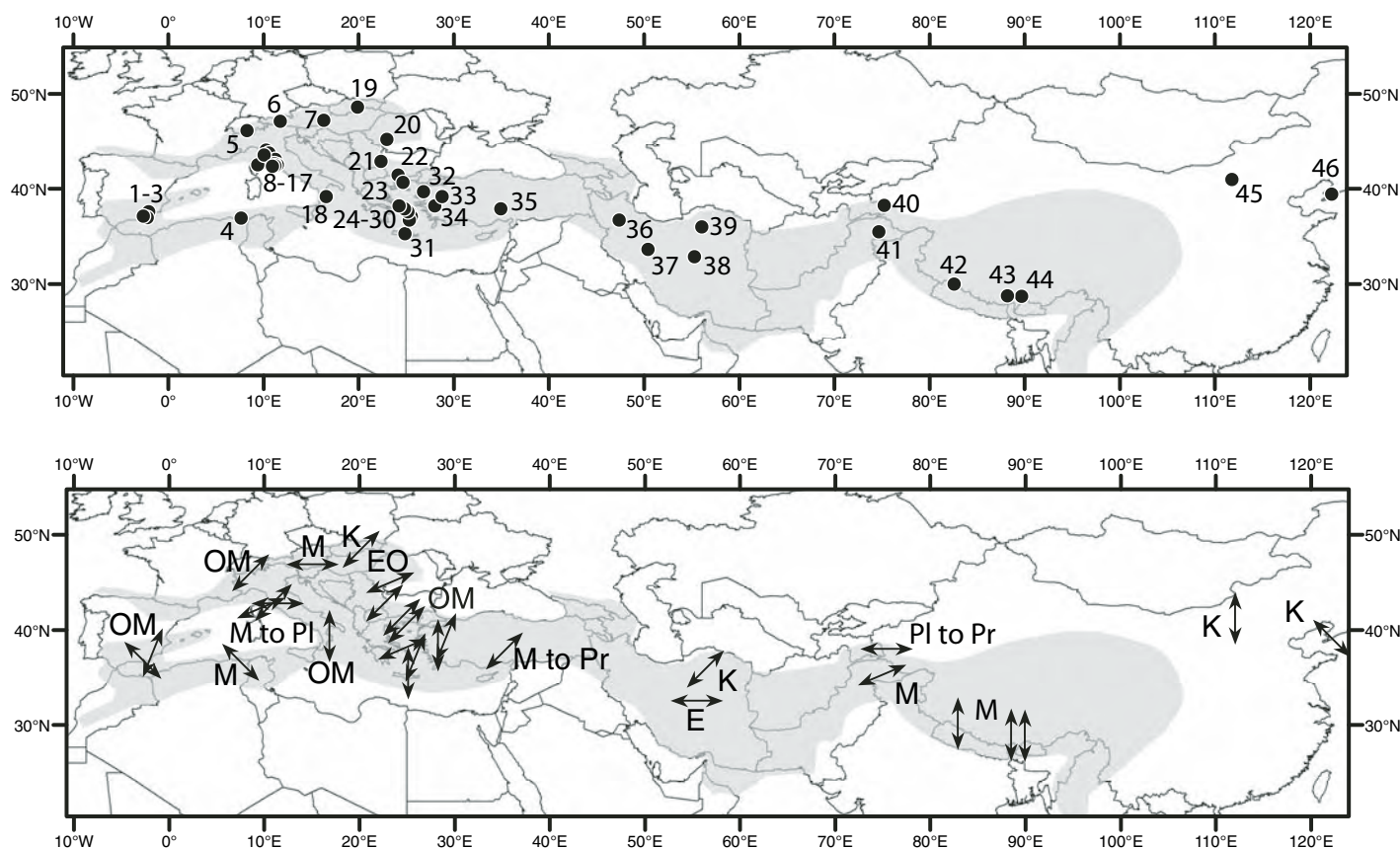


Figure 12. Map of Cretaceous to Tertiary metamorphic core complexes along the Alpine-Himalayan orogen, showing context of Iranian examples. (A) Locations of core complexes. (B) Extension directions and ages of selected core complexes. Shaded area is the approximate limit of the Tethysides, modified from Şengör (1987). K—Cretaceous, E—Eocene, O—Oligocene, M—Miocene, PI—Pliocene, Pr—Present. References in Table 1.

the Urumieh-Dokhtar magmatic arc, but perpendicular to the north-south-trending Lut segment of the Iranian arc, currently ~200 km east of the Saghand area. Kazmin et al. (1986) concluded that volcanism within the Lut arc resulted from the westward subduction of oceanic crust separating the central-east Iranian microcontinent from Afghanistan, as shown in the paleogeographic reconstructions of Dercourt et al. (1986). Eocene extension within the Saghand region therefore may be a precollisional backarc spreading event associated with the eastern segment of the Iranian arcs.

ACKNOWLEDGMENTS

We thank the University of Tehran Research Council for their support of this project and Ahmad Reza Malekpour for his efforts in the field. Ken Farley, Rebecca Flowers, and Lindsey Hedges provided assistance with the (U-Th)/He analyses. Bernard Guest and Kevin Mahan conducted informal reviews of an early version of the manuscript. Mahan also offered helpful advice in microstructural analysis. Comments

from Mark Allen, David Foster, and Uwe Ring improved the manuscript. Financial support for this project was provided by the Caltech Tectonics Observatory and National Science Foundation grant EAR-0511054.

REFERENCES CITED

- Alavi, M., 1991, Sedimentary and structural characteristics of the Paleogene remnant in northeastern Iran: *Geological Society of America Bulletin*, v. 103, p. 983–992, doi: 10.1130/0016-7606(1991)103<0983:SASCOT>2.3.CO;2.
- Argles, T.W., and Edwards, M.A., 2002, First evidence for high-grade, Himalayan-age synconvergent extension recognized within the western syntaxis; Nanga Parbat, Pakistan: *Journal of Structural Geology*, v. 24, p. 1327–1344, doi: 10.1016/S0191-8141(01)00136-5.
- Armstrong, R.L., 1982, Cordilleran metamorphic core complexes; from Arizona to southern Canada: *Annual Review of Earth and Planetary Sciences*, v. 10, p. 129–154, doi: 10.1146/annurev.ea.10.050182.001021.
- Armstrong, R.L., and Ward, P.L., 1991, Evolving geographic patterns of Cenozoic magmatism in the North American Cordillera; the temporal and spatial association of magmatism and metamorphic core complexes: *Journal of Geophysical Research, B, Solid Earth and Planets*, v. 96, p. 13,201–13,224.
- Axen, G.J., Bartley, J.M., and Selverstone, J., 1995, Structural expression of a rolling hinge in the footwall of the Brenner Line normal fault, eastern Alps: *Tectonics*, v. 14, p. 1380–1392, doi: 10.1029/95TC02406.
- Axen, G.J., Lam, P.S., Grove, M., Stockli, D.F., and Hasanzadeh, J., 2001, Exhumation of the west-central Alborz Mountains, Iran, Caspian subsidence, and collision-related tectonics: *Geology*, v. 29, p. 559–562, doi: 10.1130/0091-7613(2001)029<0559:EOTWCA>2.0.CO;2.
- Brun, J.-P., Sokoutis, D., and van den Driessche, J., 1994, Analogue modeling of detachment fault systems and core complexes: *Geology*, v. 22, p. 319–322, doi: 10.1130/0091-7613(1994)022<0319:AMODFS>2.3.CO;2.
- Brunel, M., Arnaud, N., Tapponnier, P., Pan, Y., and Wang, Y., 1994, Kongur Shan normal fault: Type example of mountain building assisted by extension (Karakoram fault, eastern Pamir): *Geology*, v. 22, p. 707–710, doi: 10.1130/0091-7613(1994)022<0707:KSNFTE>2.3.CO;2.
- Brunet, C., Monie, P., Jolivet, L., and Cadet, J.-P., 2000, Migration of compression and extension in the Tyrrhenian Sea, insights from $^{40}\text{Ar}/^{39}\text{Ar}$ ages on micas along a transect from Corsica to Tuscany: *Tectonophysics*, v. 321, p. 127–155, doi: 10.1016/S0040-1951(00)00067-6.
- Buick, I.S., 1991, The late Alpine evolution of an extensional shear zone, Naxos, Greece: *Geological Society [London] Journal*, v. 148, p. 93–103.
- Burchfiel, B.C., Chen, Z., Hodges, K.V., Yüping, L., Royden, L.H., Changrong, D., and Jiene, X., 1992, The South Tibetan detachment system, Himalayan orogen; extension contemporaneous with and parallel to shortening in a collisional mountain belt: *Geological Society of America Special Paper* 269, 41 p.
- Caby, R., Hammor, D., and Delor, C., 2001, Metamorphic evolution, partial melting and Miocene exhumation of lower crust in the Edough metamorphic core complex, west Mediterranean orogen, eastern Algeria: *Tectonophysics*, v. 342, p. 239–273, doi: 10.1016/S0040-1951(01)00166-4.

- Carmignani, L., and Roy, K., 1990, Crustal extension in the Northern Apennines; the transition from compression to extension in the Alpi Apuane core complex: *Tectonics*, v. 9, p. 1275–1303.
- Carmignani, L., Decandia, F.A., Fantozzi, P.L., Lazzarotto, A., Liotta, D., and Meccheri, M., 1994, Tertiary extensional tectonics in Tuscany (Northern Apennines, Italy): *Tectonophysics*, v. 238, p. 295–315, doi: 10.1016/0040-1951(94)90061-2.
- Chen, Z., Liu, Y., Hodges, K.V., Burchfiel, B.C., Royden, L.H., and Deng, C., 1990, The Kangmar Dome; a metamorphic core complex in southern Xizang (Tibet): *Science*, v. 250, p. 1552–1556, doi: 10.1126/science.250.4987.1552.
- Coney, P.J., 1980, Cordilleran metamorphic core complexes; an overview, *in* Crittenden, M.D., Jr., et al., eds., *Cordilleran metamorphic core complexes*: Geological Society of America Memoir 153, p. 7–31.
- Davis, G.A., and Lister, G.S., 1988, Detachment faulting in continental extension; perspectives from the Southwestern U.S. Cordillera, *in* Clark, S.P., et al., eds., *Processes in continental lithospheric deformation*: Geological Society of America Special Paper 218, p. 133–159.
- Davis, G.A., Anderson, J.L., Frost, E.G., and Shackelford, T.J., 1980, Mylonitization and detachment faulting in the Whipple-Bucks-Rawhide Mountains terrane, southeastern California and western Arizona, *in* Crittenden, M.D., Jr., et al., eds., *Cordilleran metamorphic core complexes*: Geological Society of America Memoir 153, p. 79–129.
- Davis, G.A., Darby, B.J., Yadong, Z., and Spell, T.L., 2002, Geometric and temporal evolution of an extensional detachment fault, Hohhot metamorphic core complex, Inner Mongolia, China: *Geology*, v. 30, p. 1003–1006, doi: 10.1130/0091-7613(2002)030<1003:GATEOA>2.0.CO;2.
- Davis, G.A., 1980, Structural characteristics of metamorphic core complexes, southern Arizona, *in* Crittenden, M.D., Jr., et al., eds., *Cordilleran metamorphic core complexes*: Geological Society of America Memoir 153, p. 35–77.
- Davis, G.H., and Coney, P.J., 1979, Geologic development of the Cordilleran metamorphic core complexes: *Geology*, v. 7, p. 120–124, doi: 10.1130/0091-7613(1979)7<120:GDOTCM>2.0.CO;2.
- Dercourt, J., Zonenshain, L.P., Ricou, L.E., Kazmin, V.G., Le Pichon, X., Knipper, A.L., Grandjacquet, C., Shorshikov, I.M., Geyssant, J., Lepvrier, C., Pecheurs, D.H., Boulin, J., Sibuet, J.-C., Savostin, L.A., Sorokhtin, O., Westphal, M., Bazhenov, M.L., Lauer, J.P., and Biju-Duval, B., 1986, Geological evolution of the Tethys belt from the Atlantic to the Pamirs since the Lias: *Tectonophysics*, v. 123, p. 241–315, doi: 10.1016/0040-1951(86)90199-X.
- Dewey, J.F., 1988, Extensional collapse of orogens: *Tectonics*, v. 7, p. 1123–1139.
- Dinter, D.A., 1998, Late Cenozoic extension of the Alpine collisional orogen, northeastern Greece: Origin of the north Aegean basin: *Geological Society of America Bulletin*, v. 110, p. 1208–1230, doi: 10.1130/0016-7606(1998)110<1208:LCEOTA>2.3.CO;2.
- Dinter, D.A., Macfarlane, A., Hames, W., Isachsen, C., Bowring, S., and Royden, L., 1995, U-Pb and $^{40}\text{Ar}/^{39}\text{Ar}$ geochronology of the Symvolon granodiorite: Implications for the thermal and structural evolution of the Rhodope metamorphic core complex, northeastern Greece: *Tectonics*, v. 14, p. 886–908, doi: 10.1029/95TC00926.
- Fitzgerald, P.G., Fryxell, J.E., and Wernicke, B.P., 1991, Miocene crustal extension and uplift in southeastern Nevada; constraints from fission track analysis: *Geology*, v. 19, p. 1013–1016, doi: 10.1130/0091-7613(1991)019<1013:MCEAUL>2.3.CO;2.
- Forster, H., Fesefeldt, K., and Kursten, M., 1972, Magmatic and orogenic evolution of the central Iranian volcanic belt: *International Geologic Congress*, 24th, Section 2, p. 198–210.
- Foster, D.A., Gleadow, J.W., Reynolds, S.J., and Fitzgerald, P.G., 1993, Denudation of metamorphic core complexes and the reconstruction of the transition zone, west-central Arizona: Constraints from apatite fission track thermochronology: *Journal of Geophysical Research*, v. 98, no. B2, p. 2167–2185.
- Fournier, M., Jolivet, L., Goffe, B., and Dubois, R., 1991, Alpine Corsica metamorphic core complex: *Tectonics*, v. 10, p. 1173–1186.
- Friedmann, S.J., Davis, G.A., Fowler, T.K., Brudos, T., Parke, M., Burbank, D.W., and Burchfiel, B.C., 1994, Stratigraphy and gravity-glide elements of a Miocene supradetachment basin, Shadow Valley, East Mojave Desert, *in* McGill, S.F., and Ross, T.M., eds., *Geological investigations of an active margin*: Geological Society of America Cordilleran Section guidebook: Redlands, California, Sand Bernardino County Museum Association, p. 302–318.
- Fugenschuh, B., and Schmid, S.M., 2005, Age and significance of core complex formation in a very curved orogen: Evidence from fission track studies in the South Carpathians (Romania): *Tectonophysics*, v. 404, p. 33–53, doi: 10.1016/j.tecto.2005.03.019.
- Gans, P.B., and Bohrsen, W.A., 1998, Suppression of volcanism during rapid extension in the Basin and Range Province, United States: *Science*, v. 279, p. 66–68, doi: 10.1126/science.279.5347.66.
- Gautier, P., and Brun, J.-P., 1994, Crustal-scale geometry and kinematics of late-orogenic extension in the central Aegean (Cyclades and Evvia Island): *Tectonophysics*, v. 238, p. 399–424, doi: 10.1016/0040-1951(94)90066-3.
- Gessner, K., Ring, U., Johnson, C., Hetzel, R., Passchier, C.W., and Gungor, T., 2001, An active bivergent rolling-hinge detachment system: Central Menderes metamorphic core complex in western Turkey: *Geology*, v. 29, p. 611–614, doi: 10.1130/0091-7613(2001)029<0611:AABRHD>2.0.CO;2.
- Grassl, H., Neubauer, F., Millahn, K., and Weber, F., 2004, Seismic image of the deep crust at the eastern margin of the Alps (Austria): Indications for crustal extension in a convergent orogen: *Tectonophysics*, v. 380, p. 105–122, doi: 10.1016/j.tecto.2003.12.003.
- Haghipour, A., 1977a, Geological map of the Biabanak-Bafq area: Tehran, Geological Survey of Iran, scale 1:500,000.
- Haghipour, A., 1977b, Geological map of the Posht-e-Badam area: Tehran, Geological Survey of Iran, scale 1:100,000.
- Haghipour, A., and Aghanabati, A., compilers, 1985, Geological map of Iran: Geological Survey of Iran Ministry of Mines and Metals, scale 1:2,500,000.
- Haghipour, A., Valeh, N., Pelissier, G., and Davoudzadeh, M., 1977, Explanatory text of the Ardekan quadrangle map: Geological Survey of Iran Geological Quadrangle H8, 114 p.
- Harrison, T.M., Duncan, I., and McDougall, I., 1985, Diffusion of ^{40}Ar in biotite: Temperature, pressure and compositional effects: *Geochimica et Cosmochimica Acta*, v. 49, p. 2461–2468, doi: 10.1016/0016-7037(85)90246-7.
- Hassanzadeh, J., Ghazi, A.M., Axen, G., and Guest, B., 2002, Oligo-Miocene mafic-alkaline magmatism in north and northwest of Iran: Evidence for the separation of the Alborz from the Urumieh-Dokhtar magmatic arc: *Geological Society of America Abstracts with Programs*, v. 34, no. 6, p. 331.
- Hassanzadeh, J., Malekpour, A., Grove, M., Axen, G.J., Horton, B.K., Stockli, D.F., Farley, K., Schmitt, A.K., Mohajjel, M., and Ghazi, A.M., 2005, Biarmid metamorphic core complex; new evidence for Late Cretaceous–Paleocene extensional tectonics along the northern margin of central Iranian Plateau: *Geological Society of America Abstracts with Programs*, v. 37, no. 7, p. 71.
- Hippert, J., and Tohver, E., 1999, On the development of zones of reverse shearing in mylonitic rocks: *Journal of Structural Geology*, v. 21, p. 1603–1614, doi: 10.1016/S0191-8141(99)00107-8.
- Hodges, K.V., McKenna, L.W., Stock, J., Knapp, J., Page, L., Sternlof, K., Wuest, G., and Walker, J.D., 1989, Evolution of extensional basins and basin and range topography west of Death Valley, California: *Tectonics*, v. 8, p. 453–467.
- Holm, D.K., and Dokka, R.K., 1993, Interpretation and tectonic implications of cooling histories; an example from the Black Mountains, Death Valley extended terrane, California: *Earth and Planetary Science Letters*, v. 116, p. 63–80, doi: 10.1016/0012-821X(93)90045-B.
- House, M.A., Farley, K.A., and Stockli, D., 2000, Helium chronometry of apatite and titanite using Nd-YAG laser heating: *Earth and Planetary Science Letters*, v. 183, p. 365–368, doi: 10.1016/S0012-821X(00)00286-7.
- Hubbard, M.S., Spencer, D.A., and West, D.P., 1995, Tectonic exhumation of the Nanga Parbat massif, northern Pakistan: *Earth and Planetary Science Letters*, v. 133, p. 213–225, doi: 10.1016/0012-821X(95)00075-N.
- Jaffey, A.H., Flynn, K.F., Glendenin, L.E., Bentley, W.C., and Essling, A.M., 1971, Precision measurement of half-lives and specific activities of ^{235}U and ^{238}U : *Physical Review C*, v. 4, p. 1889–1906, doi: 10.1103/PhysRevC.4.1889.
- Janak, M., Plasienska, D., Frey, M., Cosca, M., Schmidt, S.T., Luptak, B., and Mercs, S., 2001, Cretaceous evolution of a metamorphic core complex, the Veporic unit, Western Carpathians (Slovakia): *P-T* conditions and in situ $^{40}\text{Ar}/^{39}\text{Ar}$ UV laser probe dating of metapelites: *Journal of Metamorphic Geology*, v. 19, p. 197–216, doi: 10.1046/j.0263-4929.2000.00304.x.
- John, B.E., 1987, Structural and intrusive history of the Chemehuevi Mountains area, southeastern California and western Arizona [Ph.D. thesis]: Santa Barbara, University of California, 344 p.
- Jolivet, L., Faccenna, C., Goffe, B., Mattei, M., Rossetti, F., Brunet, C., Storti, F., Funiciello, R., Cadet, J.P., d'Agostino, N., and Parra, T., 1998, Midcrustal shear zones in post-orogenic extension: Example from the northern Tyrrhenian Sea: *Journal of Geophysical Research*, v. 103, p. 12,123–12,160, doi: 10.1029/97JB03616.
- Liu, Junlai, Davis, G.A., Zhiyong, L., and Fuyuan, W., 2005, The Liaonan metamorphic core complex, Southeastern Liaoning Province, North China: A likely contributor to Cretaceous rotation of Eastern Liaoning, Korea, and contiguous areas: *Tectonophysics*, v. 407, p. 65–80, doi: 10.1016/j.tecto.2005.07.001.
- Kargaran, F., Neubauer, F., Genser, J., and Houshmandzadeh, A., 2006, The Eocene Chapedony metamorphic core complex in central Iran: Preliminary structural results: *European Geosciences Union Geophysical Research Abstracts*, v. 8.
- Kazmin, V.G., Shorshikov, I.M., Ricou, L.-E., Zonenshain, L.P., Boulin, J., and Knipper, A.L., 1986, Volcanic belts as markers of the Mesozoic–Cenozoic active margin of Eurasia: *Tectonophysics*, v. 123, p. 123–152, doi: 10.1016/0040-1951(86)90195-2.
- Kounov, A., Seward, D., Bernoulli, D., Burg, J.-P., and Ivanov, Z., 2004, Thermotectonic evolution of an extensional dome: The Cenozoic Osovo-Lisets core complex (Kraishte zone, western Bulgaria): *Geologische Rundschau*, v. 93, p. 1008–1024.
- Kumerics, C., Ring, U., Bricchau, S., Glodny, J., and Monie, P., 2005, The extensional Messaria shear zone and associated brittle detachment faults, Aegean Sea, Greece: *Geological Society [London] Journal*, v. 162, p. 701–721, doi: 10.1144/0016-764904-041.
- Lee, J., and Lister, G.S., 1992, Late Miocene ductile extension and detachment faulting, Mykonos, Greece: *Geology*, v. 20, p. 121–124, doi: 10.1130/0091-7613(1992)020<0121:LMDEAD>2.3.CO;2.
- Lee, J., Miller, E.L., and Sutter, J.F., 1987, Ductile strain and metamorphism in an extensional tectonic setting: A case study from the northern Snake Range, Nevada, USA, *in* Coward, M.P., et al., eds., *Continental extensional tectonics*: Geological Society [London] Special Publication 28, p. 267–298.
- Lee, J., Hacker, B.R., Dinklage, W.S., Wang, Y., Gans, P., Calvert, A., Wan, J., Chen, W., Blythe, A.E., and McClelland, W., 2000, Evolution of the Kangmar Dome, southern Tibet: Structural, petrologic and thermochronologic constraints: *Tectonics*, v. 19, p. 872–895, doi: 10.1029/1999TC001147.
- Lee, J., Hacker, B., and Wang, Y., 2004, Evolution of north Himalayan gneiss domes: Structural and metamorphic studies in Mabja Dome, southern Tibet: *Journal of Structural Geology*, v. 26, p. 2297–2316, doi: 10.1016/j.jsg.2004.02.013.
- Lehrmann, D.J., Ramezani, J., Bowring, S.A., Martin, M.W., Montgomery, P., Enos, P., Payne, J.L., Orchard, M.J., Wang, H., and Wei, J., 2006, Timing of recovery from the end-Permian extinction: geochronologic and biostratigraphic constraints from south China: *Geology*, v. 34, p. 1053–1056, doi: 10.1130/G22827A.1.
- Lister, G.S., Banga, G., and Feenstra, A., 1984, Metamorphic core complexes of Cordilleran type in the Cyclades, Aegean Sea, Greece: *Geology*, v. 12, p. 221–225, doi: 10.1130/0091-7613(1984)12<221:MCCOCT>2.0.CO;2.
- Lonergan, L., and White, N., 1997, Origin of the Betic-Rif mountain belt: *Tectonics*, v. 16, p. 504–522, doi: 10.1029/96TC03937.
- Ludwig, K.R., 1980, Calculation of uncertainties of U-Pb isotope data: *Earth and Planetary Science Letters*, v. 46, p. 212–220, doi: 10.1016/0012-821X(80)90007-2.

- MacCready, T., Snoko, A.W., Wright, J.E., and Howard, K.A., 1997, Mid-crustal flow during Tertiary extension in the Ruby Mountains core complex, Nevada: Geological Society of America Bulletin, v. 109, p. 1576–1594, doi: 10.1130/0016-7606(1997)109<1576:MCFDTE>2.3.CO;2.
- Mancktelow, N.S., and Pavlis, T.L., 1994, Fold-fault relationships in low-angle detachment systems: Tectonics, v. 13, p. 668–685, doi: 10.1029/93TC03489.
- McQuarrie, N., Stock, J.M., Verdel, C., and Wernicke, B.P., 2003, Cenozoic evolution of Neotethys and implications for the causes of plate motions: Geophysical Research Letters, v. 30, p. 2036, doi: 10.1029/2003GL017992.
- Niemi, N.A., Wernicke, B.P., Brady, R.J., Saleeby, J.B., and Dunne, G.C., 2001, Distribution and provenance of the middle Miocene Eagle Mountain Formation, and implications for regional kinematic analysis of the Basin and Range Province: Geological Society of America Bulletin, v. 113, p. 419–442, doi: 10.1130/0016-7606(2001)113<0419:DAPOTM>2.0.CO;2.
- Noble, L.F., 1941, Structural features of the Virgin Spring area, Death Valley, California: Geological Society of America Bulletin, v. 52, p. 941–999.
- Okay, A.I., and Satir, M., 2000, Coeval plutonism and metamorphism in a latest Oligocene metamorphic core complex in northwest Turkey: Geological Magazine, v. 137, p. 495–516, doi: 10.1017/S0016756800004532.
- Passchier, C.W., and Trouw, R.A.J., 2005, Microtectonics: Berlin, Springer, 366 p.
- Platt, J.P., and Compagnoni, R., 1990, Alpine ductile deformation and metamorphism in a Calabrian basement nappe (Aspromonte, South Italy): Eclogae Geologicae Helveticae, v. 83, p. 41–58.
- Platt, J.P., and Vissers, R.L.M., 1989, Extensional collapse of thickened continental lithosphere: A working hypothesis for the Alboran sea and Gibraltar arc: Geology, v. 17, p. 540–543, doi: 10.1130/0091-7613(1989)017<0540:ECOTCL>2.3.CO;2.
- Platzman, E., and Platt, J.P., 2004, Kinematics of a twisted core complex: Oblique axis rotation in an extended terrane (Betic Cordillera, southern Spain): Tectonics, v. 23, p. TC6010, doi: 10.1029/2003TC001549.
- Ramezani, J., and Tucker, R.D., 2003, The Saghand region, central Iran: U-Pb geochronology, petrogenesis and implications for Gondwana tectonics: American Journal of Science, v. 303, p. 622–665, doi: 10.2475/aj.s.303.7.622.
- Ratschbacher, L., Behrmann, J.H., and Pahr, A., 1990, Penninic windows at the eastern end of the Alps and their relation to the intra-Carpathian basins: Tectonophysics, v. 172, p. 91–105, doi: 10.1016/0040-1951(90)90061-C.
- Ratschbacher, L., Merle, O., Davy, P., and Cobbold, P., 1991a, Lateral extrusion in the eastern Alps, part I, boundary conditions and experiments scaled for gravity: Tectonics, v. 10, p. 245–256.
- Ratschbacher, L., Frisch, W., and Linzer, H.-G., 1991b, Lateral extrusion in the eastern Alps, part II, structural analysis: Tectonics, v. 10, p. 257–271.
- Rehrig, W.A., and Reynolds, S.J., 1980, Geologic and geochronologic reconnaissance of a northwest-trending zone of metamorphic core complexes in southern and western Arizona, in Crittenden, M.D., Jr., et al., eds., Cordilleran metamorphic core complexes: Geological Society of America Memoir 153, p. 131–157.
- Reiners, P.W., Brady, R., Farley, K.A., Fryxell, J.E., Wernicke, B., and Lux, D., 2000, Helium and argon thermochronometry of the Gold Butte block, South Virgin Mountains, Nevada: Earth and Planetary Science Letters, v. 178, p. 315–326, doi: 10.1016/S0012-821X(00)00080-7.
- Reiners, P.W., Farley, K.A., and Hickes, H.J., 2002, He diffusion and (U-Th)/He thermochronometry of zircon: initial results from Fish Canyon Tuff and Gold Butte: Tectonophysics, v. 349, p. 297–308, doi: 10.1016/S0040-1951(02)00058-6.
- Renne, P.R., Swisher, C.C., Deino, A.L., Karner, D.B., Owens, T., and DePaolo, D.J., 1998, Intercalibration of standards, absolute ages and uncertainties in $^{40}\text{Ar}/^{39}\text{Ar}$ dating: Chemical Geology, v. 145, p. 117–152, doi: 10.1016/S0009-2541(97)00159-9.
- Reynolds, S.J., 1985, Geology of the South Mountains, central Arizona: Arizona Bureau of Geology and Mineral Technology, Geological Survey Branch, Bulletin 195, 61 p.
- Ring, U., and Collins, A.S., 2005, U-Pb SIMS dating of syn-kinematic granites: Timing of core-complex formation in the northern Anatolide belt of western Turkey: Geological Society [London] Journal, v. 162, p. 289–298, doi: 10.1144/0016-764904-016.
- Ring, U., Thomson, S.N., and Brocker, M., 2003, Fast extension but little exhumation: The Vari detachment in the Cyclades, Greece: Geological Magazine, v. 140, p. 245–252, doi: 10.1017/S0016756803007799.
- Royden, L.H., 1993, Evolution of retreating subduction boundaries formed during continental collision: Tectonics, v. 12, p. 629–638.
- Schmid, S.M., Berza, T., Diaconescu, V., Froitzheim, N., and Fugenschuh, B., 1998, Orogen-parallel extension in the Southern Carpathians: Tectonophysics, v. 297, p. 209–228, doi: 10.1016/S0040-1951(98)00169-3.
- Schoene, B., Crowley, J.L., Condon, D.J., Schmitz, M.D., and Bowring, S.A., 2006, Reassessing the uranium decay constants for geochronology using ID-TIMS U-Pb data: Geochimica et Cosmochimica Acta, v. 70, p. 426–445, doi: 10.1016/j.gca.2005.09.007.
- Şengör, A.M.C., 1987, Tectonics of the Tethysides; orogenic collage development in a collisional setting: Annual Review of Earth and Planetary Sciences, v. 15, p. 213–244, doi: 10.1146/annurev.ea.15.050187.001241.
- Şengör, A.M.C., and Natal'in, B.A., 1996, Paleotectonics of Asia: Fragments of a synthesis, in Yin, A., and Harrison, M., The tectonic evolution of Asia: Cambridge, Cambridge University Press, p. 486–640.
- Shackelford, T.J., 1980, Tertiary tectonic denudation of a Mesozoic-early Tertiary(?) gneiss complex, Rawhide Mountains, western Arizona: Geology, v. 8, p. 190–194, doi: 10.1130/0091-7613(1980)8<190:TTDOAM>2.0.CO;2.
- Soffel, H.C., Davoudzadeh, M., Rolf, C., and Schmidt, S., 1996, New palaeomagnetic data from central Iran and a Triassic palaeoreconstruction: Geologische Rundschau, v. 85, p. 293–302.
- Spencer, J.E., and Reynolds, S.J., 1989, Middle Tertiary tectonics of Arizona and adjacent areas: Arizona Geological Society Digest, v. 17, p. 539–574.
- Spencer, J.E., and Welly, J.W., 1986, Possible controls of base- and precious-metal mineralization associated with Tertiary detachment faults in the lower Colorado River trough, Arizona and California: Geology, v. 14, p. 195–198, doi: 10.1130/0091-7613(1986)14<195:PCOBAP>2.0.CO;2.
- Stockli, D.F., 2005, Application of low-temperature thermochronometry to extensional tectonic settings: Reviews in Mineralogy and Geochemistry, v. 58, p. 411–448, doi: 10.2138/rmg.2005.58.16.
- Stockli, D.F., Hassanzadeh, J., Stockli, L.D., Axen, G.J., Walker, J.D., and Dewane, T.J., 2004, Structural and geochronological evidence for Oligo-Miocene intra-arc low-angle detachment faulting in the Takab-Zanjan area, NW Iran: Geological Society of America Abstracts with Programs, v. 36, no. 5, p. 319.
- Stöcklin, J., 1968, Structural history and tectonics of Iran: A review: American Association of Petroleum Geologists Bulletin, v. 52, p. 1229–1258.
- Tagami, T., Farley, K.A., and Stockli, D.F., 2003, (U-Th)/He geochronology of single zircon grains of known Tertiary eruption age: Earth and Planetary Science Letters, v. 207, p. 57–67, doi: 10.1016/S0012-821X(02)01144-5.
- Takin, M., 1972, Iranian geology and continental drift in the Middle East: Nature, v. 235, p. 147–150, doi: 10.1038/235147a0.
- Thiele, O., Alavi, M., Assefi, R., Hushmand-zadeh, A., Sayed-Emami, K., and Zahedi, M., 1967, Geological map of Golpaygan: Tehran, Geological Survey of Iran, scale 1:250,000.
- Thomson, S.N., 1994, Fission track analysis of the crystalline basement rocks of the Calabrian Arc, southern Italy: evidence of Oligo-Miocene late-orogenic extension and erosion: Tectonophysics, v. 238, p. 331–352, doi: 10.1016/0040-1951(94)90063-9.
- Thomson, S.N., Stoeckert, B., and Brix, M.R., 1999, Miocene high-pressure metamorphic rocks of Crete, Greece; rapid exhumation by buoyant escape, in Ring, U., et al., eds., Exhumation processes: Normal faulting, ductile flow and erosion: Geological Society [London] Special Publication 154, p. 87–107.
- Tillman, J.E., Poosti, A., Rossello, S., and Eckert, A., 1981, Structural evolution of Sanandaj-Sirjan Ranges near Esfahan, Iran: American Association of Petroleum Geologists Bulletin, v. 65, p. 674–687.
- Valeh, N., and Haghipour, A., 1970, Geological map of Ardekan: Tehran, Geological Survey of Iran, scale 1:250,000.
- van Hinsbergen, D.J.J., and Meulenkamp, J.E., 2006, Neogene supradetachment basin development on Crete (Greece) during exhumation of the South Aegean core complex: Basin Research, v. 18, p. 103–124, doi: 10.1111/j.1365-2117.2005.00282.x.
- Vincent, S.J., Allen, M.B., Ismail-Zadeh, A.D., Flecker, R., Foland, K.A., and Simmons, M.D., 2005, Insights from the Talysh of Azerbaijan into the Paleogene evolution of the south Caspian region: Geological Society of America Bulletin, v. 117, p. 1513–1533, doi: 10.1130/B25690.1.
- Walker, J.D., Bartley, J.M., and Glazner, A.F., 1990, Large-magnitude Miocene extension in the central Mojave Desert; implications for Paleozoic to Tertiary paleogeography and tectonics: Journal of Geophysical Research, B, Solid Earth and Planets, v. 95, p. 557–569.
- Wallis, S.R., Platt, J.P., and Knott, S.D., 1993, Recognition of syn-convergence extension in accretionary wedges with examples from the Calabrian Arc and the Eastern Alps: American Journal of Science, v. 293, p. 463–494.
- Wawrzyniec, N., and Krohe, A., 1998, Exhumation and doming of the Thasos metamorphic core complex (S Rhodes, Greece): Structural and geochronological constraints: Tectonophysics, v. 285, p. 301–332, doi: 10.1016/S0040-1951(97)00276-X.
- Wawrzyniec, T.F., Selverstone, J., and Axen, G.J., 2001, Styles of footwall uplift along the Simpol and Brenner normal fault systems, central and Eastern Alps: Tectonics, v. 20, p. 748–770, doi: 10.1029/2000TC001253.
- Wells, M.L., Snee, L.W., and Blythe, A.E., 2000, Dating of major normal fault systems using thermochronology: an example from the Raft River detachment, Basin and Range, western United States: Journal of Geophysical Research, B, Solid Earth and Planets, v. 105, p. 16,303–16,327, doi: 10.1029/2000JB009094.
- Wernicke, B., 1981, Low-angle normal faults in the Basin and Range Province: nappe tectonics in an extending orogen: Nature, v. 291, p. 645–648, doi: 10.1038/291645a0.
- Wernicke, B., 1985, Uniform-sense normal simple shear of the continental lithosphere: Canadian Journal of Earth Sciences, v. 22, p. 108–125.
- Wernicke, B., 1992, Cenozoic extensional tectonics of the U.S. Cordillera, in Burchfiel, B.C., et al., eds., The Cordilleran orogen; continuous U.S.: Boulder, Colorado, Geological Society of America, Geology of North America, v. G-3, p. 553–581.
- Wernicke, B., and Axen, G.J., 1988, On the role of isostasy in the evolution of normal fault systems: Geology, v. 16, p. 848–851, doi: 10.1130/0091-7613(1988)016<0848:OTROI>2.3.CO;2.
- Wernicke, B., and Burchfiel, B.C., 1982, Modes of extensional tectonics: Journal of Structural Geology, v. 4, p. 105–115, doi: 10.1016/0191-8141(82)90021-9.
- Whitney, D.L., and Dilek, Y., 1997, Core complex development in central Anatolia, Turkey: Geology, v. 25, p. 1023–1026, doi: 10.1130/0091-7613(1997)025<1023:CCDICA>2.3.CO;2.
- Wolf, R.A., Farley, K.A., and Silver, L.T., 1996, Helium diffusion and low-temperature thermochronometry of apatite: Geochimica et Cosmochimica Acta, v. 60, p. 4231–4240, doi: 10.1016/S0016-7037(96)00192-5.
- Wright, L.A., and Troxel, B.W., 1984, Geology of the northern half of the Confidence Hills 15-minute Quadrangle, Death Valley region, eastern California; the area of the Amargosa chaos: California Division of Mines and Geology Map Sheet, v. 34, 31 p.
- Wright, L.A., Otton, J.K., and Troxel, B.W., 1974, Turtle-back surfaces of Death Valley viewed as phenomena of extensional tectonics: Guidebook, Death Valley region, California and Nevada: Geology, v. 2, p. 53–54, doi: 10.1130/0091-7613(1974)2<53:TSODVV>2.0.CO;2.
- Yin, A., Harrison, T.M., Murphy, M.A., Grove, M., Nie, S., Ryerson, F.J., Feng, W.X., and Chen, Z.L., 1999, Tertiary deformation history of southeastern and southwestern Tibet during the Indo-Asian collision: Geological Society of America Bulletin, v. 111, p. 1644–1664, doi: 10.1130/0016-7606(1999)111<1644:TDHOSA>2.3.CO;2.

MANUSCRIPT RECEIVED 12 SEPTEMBER 2006
 REVISED MANUSCRIPT RECEIVED 1 FEBRUARY 2007
 MANUSCRIPT ACCEPTED 14 FEBRUARY 2007

Printed in the USA